NOAA Technical Memorandum NWS SR-137

MODES OF SUPERCELL INITIATION ALONG THE DRYLINE

Stephen S. Parker
National Weather Service Forecast Office
Norman, Oklahoma

Scientific Services Division
Southern Region
Fort Worth, Texas
November 1991

NITED STATES
DEPARTMENT OF COMMERCE
Robert A. Mosbacher, Secretary

National Oceanic and Atmospheric Administration
John A. Knauss
Under Secretary and Administrator

National Weather Service
Elbert W. Friday
Assistant Administrator

ACKNOWLEDGEMENTS

This technical memorandum is drawn from my recently completed Masters thesis. I would like to thank my major advisor, Dr. Howard Bluestein, for his guidance throughout this project. His insight and suggestions were invaluable. I am indebted to Don Burgess and Dr. Fred Carr for serving on my committee, and for supplying helpful insights and suggestions for my research.

I am also thankful to Dr. Meta Sienkiewicz, Mark Shafer (Wafe), and Sue Weygandt, who expertly drafted the tables and many of the figures. The meteorologists at the WSFO in Norman, where I am now employed, have been of assistance. In particular, former MIC Dr. Ken Crawford is thanked for allowing me to work on the thesis that this memo was extracted from "on the job." His successors, Larry Mooney and Dennis McCarthy, continued this philosophy and this was greatly appreciated. NSF research grants ATM-8606090 and ATM-8902594 supported this research.

TABLE OF CONTENTS

ABSTRACT

Supercells have long been recognized as producers of severe weather, and the dryline has long been recognized as a preferred region of thunderstorm (including supercell) development. However, the modes of initial formation of these dryline supercells have yet to be examined. Radar microfilm of selected dryline supercells has been studied and the following six modes of initial development have been determined: isolated; pair; line segment; cluster; merger; and squall line. Characteristics of storm evolution such as splitting, backbuilding, and the orientations of cells compared to shear vectors were also examined (through the time of severe weather occurrence).

Soundings from the proximity of each storm were used to estimate a sounding representative of the environment at the time and location of each storm's first echo. These estimated environmental soundings were then plotted (including hodographs) and many sounding and hodograph parameters (such as CAPE, BRN, LMS, etc.) were computed. The averaged data compare favorably with earlier studies of supercell storm environments. Statistical significance tests indicate that these modes are more alike than different.

A previously unstudied parameter of severe storms, the time from first echo to the time of first severe weather occurrence, has been determined for each of the storms. An overall average of 1.95 hours has been established. However, significant differences exist between certain storm modes. Specifically, the isolated and line segment modes produce severe weather in a shorter time, and pair mode storms produce severe weather in a longer time, than the average. This should be useful information to nowcasters and mesoscale modelers as they attempt to predict specific "storm day" evolutions.

MODES OF SUPERCELL FORMATION ALONG THE DRYLINE

SECTION I

INTRODUCTION

1.1 Supercells

Supercells have long been recognized as major producers of severe weather (tornadoes, hail at least three-quarters of an inch in diameter, and/or wind speeds greater than 50 knots). Although the precise definition of a supercell has been evolving through the years and is still a matter of debate, the basic structure of the supercell is well understood. Browning (1964, 1968) composed a conceptual model of supercells. He noted that these storms develop in an environment of strong vertical shear, with winds veering in direction and increasing in speed from the ground to the upper troposphere. An airflow model was devised which showed, in a storm relative sense, air entering the storm at low levels from the southeast, at mid levels from the southwest, and at upper levels from the west. Warm moist air from near the surface feeds a single large tilted updraft driven by conditional instability, and upper-level air returns to the ground in a tilted downdraft driven by the intake of dry mid-level air, evaporative cooling, and precipitation drag. These two currents do not interfere with each other, but rather work to the mutual benefit of one another. The downdraft spreads out at the surface and creates a gust front which increases convergence and helps to support the updraft.

As more data were gathered due to increases in the use of Doppler radar and in the number of storm-intercept projects, a more complete understanding of the inner workings of supercells was obtained. Lemon and Doswell (1979) synthesized and expanded on this new data set to update the supercell model. This included the importance of the rear flank downdraft, which is produced as air at upper levels is forced down the upwind side of the storm due to the convergence present there. This air is then cooled by evaporation as it mixes with unsaturated air below, and reaches the surface to the southwest of the main updraft. This is thought to play an important role in tornadogenesis. Also, the tilting of horizontal vorticity into the vertical as a source of rotation was discussed.

In the mid-1970's modelers began to simulate storms in idealized environments (e.g. Wilhelmson 1974, Miller and Pearce 1974, Schlesinger 1978). Furthermore, in the late 1970's supercell simulation became possible. Areas of modelling study include: the influence of shear-induced pressure gradients on thunderstorm motion (Rotunno and Klemp, 1982), the dependence of simulated storms on vertical wind shear and buoyancy (Weisman and Klemp, 1982), tornado production (Klemp and Rotunno, 1983), and the rotation and propagation of supercells (Rotunno and Klemp, 1985), just to give a few examples. All of these papers and many others are discussed in a review of tornadic storms in Klemp (1987).

As mentioned earlier, the precise definition of a supercell thunderstorm varies. The Lemon criteria (1977) for determination of severe storms (supercells, in particular) are not usable here because volume scans (scans consisting of a series of cross sections at increasing elevation angles) are required for analysis, whereas in this work, only 0.5

degree elevation angle scans are available. The Lemon criteria involve (among other things) the identification of a weak echo region (WER) or bounded WER (BWER) through the examination of volume scans of radar data. Lemon and Doswell (1979) discuss supercells in terms of three stages, the second of which includes the development of both a BWER and a mesocyclone. It is implied that these two phenomena must be present in order for a storm to be classified as a supercell.

The previous two definitions have been based on observational characteristics. Alternatively, the following two are based on dynamical criteria. Rotunno and Klemp (1985) list two conditions necessary for supercell classification: 1) a significant degree of organized rotation about a vertical axis, and 2) propagation to the right of the mean wind in the troposphere for periods longer than the residence time of an air parcel within the storm. Davies-Jones (1984) and Lilly (1986a and 1986b) have shown that supercell thunderstorms typically possess high degrees of helicity (the vector inner product of velocity and vorticity) and streamwise vorticity (helicity normalized by the scalar magnitude of velocity), and these could also be defining factors.

One cannot discuss supercells without acknowledging the growing support for the view that the supercell is an extreme case in a continuum of storm types (e.g., Foote and Frank 1983, Vasiloff et.al. 1986). This continuum runs from the multicell with two or more discrete cells in various stages of development to the steady-state, single updraft idealized supercell (fig. 1-1). The majority of storms in this study appear to fall into the weak evolution (Foote and Frank 1983) category, but all show signs of possessing a long-lived quasi-steady updraft at some time in their life-cycles (definitive determination of type is not possible in many cases due to the lack of extremely high resolution data).

For the purposes of this study, a storm with supercell characteristics is defined as one which is long-lived (greater than one hour), consists of a single dominant core of reflectivity for the majority of its lifetime (discrete propagation is acceptable because there are occasional gaps of up to ten minutes in low elevation angle scans in the radar microfilm), and moves to the right of the mean tropospheric wind during its mature phase (fig. 1-2). Although desirable, a definition including rotation is impossible to use in this study due to the reliance on conventional radar for data collection (see Section 2).

1.2 The Dryline

The dryline has been studied since the 1950s. Fujita (1958) and Rhea (1966) found it to be a preferred location for thunderstorm development. In the following decade, Schaefer (1974a,b) studied the life cycle and motion of the dryline. He found a dryline to be present over the south-central U.S. on all or part of just over 41% of all springtime days (April, May, and June) over the period 1966-1968. This phenomenon is also found in other areas of the world, such as Africa, India (Weston 1973), and China (Golden 1980); however this study will only address the dryline in the Southern Plains of the United States.

A dryline is a zone of strong moisture gradient at the surface (fig. 1-3). It is nearly vertical from the surface to a height of typically one to two km, and then slopes sharply back over the moist surface air. It is formed when hot, dry air from the Mexican Plateau forms a cap or lid on top of warm, moist air flowing northward from the Gulf of Mexico (Carlson and Ludlum, 1968). Due to the sloping terrain of the South Plains, the moisture is deeper to the east and more shallow to the west. As the sun heats the air west of the dryline, a nearly dry-adiabatic lapse rate results and this allows mixing of momentum and moisture to occur over a deep layer of the lower troposphere. As relatively strong winds move over the shallow layer of moisture just east of the dryline,

the dry air reaches the surface through turbulent mixing and diffuses the moisture in the vertical. Thus the dryline appears to "move" eastward - sometimes even appearing to "jump" a considerable distance in a short period of time. Eventually, the dryline encounters a layer of moisture that is too deep to mix out and/or solar insolation is lessened as the afternoon wears on, and the dryline stalls. At night, the dryline tends to recede westward as a nocturnal inversion develops and surface layer winds decouple from the low level jet.

Present understanding of how the dryline initiates convection is incomplete. One theory, recently disproven, has been that buoyancy maxima were created through non-linear biconstituent diffusion (Schaefer, 1975). In short, it was believed that hotter, drier air on the west side and cooler, moister air on the east side mix in the zone of greatest moisture gradient to produce a maximum in virtual temperature, and therefore positive buoyancy. If this amount of buoyancy is sufficient to overcome the capping inversion, storms would form. Recently, however, Lilly and Gal-Chen (1990) have shown that this process actually produces a minimum in potential buoyancy. It is therefore not a likely candidate for a trigger mechanism. Note: a trigger mechanism is any forcing which is sufficient to break a capping inversion and thereby initiate convection. Examples of potential trigger mechanisms include low level moisture convergence, symmetric instability, a low level jet, and "dry" convergence, due simply to a westerly component of wind on the west side of the dryline and an easterly one on the east. Convergence (including moisture convergence) may be locally enhanced by dryline waves or bulges, as hypothesized by Tegtemeier (1974) and shown to exist by, e.g., McCarthy and Koch (1982). Symmetric instability (McGinley and Sasaki 1975) is thought to occur in the air west of the dryline as Richardson numbers (Ri) reach a critical range (from 0.25 to 1.0). Symmetric instability aids in the downward transport of high momentum westerlies and results in an increase in the eastward motion of the dryline, which in turn should increase convergence. Davies-Jones and Zacharias (1988) analyzed waves on the dryline in Kansas for the 10 May 1985 tornado outbreak and considered symmetric instability as a source mechanism for the waves. However, further study by Davies-Jones and Zacharias (unpublished - personal communication with Davies-Jones) concluded that this could not have been the source, and no specific source has yet been identified.

1.3 Environmental Soundings

Environmental soundings have seen much use over the years, generally in attempting to determine what atmospheric qualities are conducive to tornado formation. Environmental soundings are defined as those within an arbitrarily given distance and time period of an event in question. Fawbush and Miller (1952) were perhaps the first to use them, with other notable studies such as Beebe (1958), Wills (1969), Darkow (1969), and Maddox (1976) to follow. Maddox (1976) determined that the small-scale storm environment cannot be determined from environmental soundings.

Environmental soundings were also used in this study, but of a slightly different type to those mentioned above. As in Bluestein and Jain (1985) and Bluestein et. al. (1987), soundings were interpolated in time and space. In this study, the interpolation was done to determine the conditions at the time and location of the storms' first radar return (echo), hereafter referred to as FE. Soundings were then grouped by initial modes (see Section 3) similar to the Blanchard (1990) groupings of MCS (Mesoscale Convective System) types.

1.4 Overview

This study is a climatology of convective storms which formed on or very near the dryline, exhibited supercell characteristics, and produced severe weather as recorded in Storm Data. Radar microfilm, mainly from the National Severe Storm Laboratory (NSSL) Weather Surveillance Radar (WSR) 57, was used to document each storm's lifecycle from FE. This type of radar microfilm survey was also employed by Houze et. al. (1990), Bluestein and Jain (1985) and Bluestein et. al. (1987).

The purpose of this research is to document the occurrence of severe thunderstorms with supercell characteristics that develop along or just ahead of the dryline and categorize their modes of formation. These modes will then be related to the environmental soundings constructed for each storm, and to storm characteristics throughout the development of the storm. Also, the time from FE to the first occurrence of severe weather (as reported in Storm Data) will be documented as well as data on storm intensity and motion. This study fills the need for a climatology of supercells which form on or just ahead the dryline. It will serve as a basis for comparison with future numerical simulations of the initial phases of storm development. The documentation of the time from FE to first severe weather occurrence should aid nowcasters and mesoscale modelers. Finally, it is an attempt to view the overall developmental picture of this type of storm as opposed to the numerous case studies which have been done.

SECTION II

DATA AND METHODOLOGY

The data used in this study included the following: Storm Data (SD); the NSSL WSR-57 radar microfilm library; selected National Weather Service (NWS) radar microfilm from Oklahoma City, Amarillo, and Stephenville, Texas; radar tracings of NWS radar microfilm from Garden City, Kansas; soundings from the National Center for Atmospheric Research (NCAR) sounding data base; special soundings from the National Severe Storm Laboratory (NSSL) and from University of Oklahoma (OU) storm intercept operations; three-hourly surface maps; and numerous Spring Summaries from NSSL.

Potential cases during the period 1971-1986 on which severe storms may have occurred on or near the dryline in the Southern Plains, particularly in Oklahoma, the Texas Panhandle, and North-central Texas, were compiled by searching SD for the months of March through June. For the purposes of this work, severe weather is defined as those events listed in SD: hail greater than or equal to three-quarters of an inch in diameter; winds greater than or equal to 50 kts; tornadoes; and funnel clouds (even though the NWS definition does not include funnel clouds). Surface maps were examined and in many cases reanalyzed to determine if a dryline was in the vicinity of thunderstorm development. Radar microfilm was then reviewed (pictures were usually available every one to five minutes at 0.5 degrees elevation angle) to discover the exact time and location of each storm's FE at that elevation angle. These were then compared with the surface maps closest in time to determine whether or not the storm developed on or ahead (within approximately 100 km) of the dryline. In Oklahoma, a total of 23 days had storms for which the following conditions were met: 1) severe storms occurred on or near a dryline, and 2) microfilm data were available from FE until the time of the first severe report. In Texas there were eleven days, and in Kansas there was only one day (this study was originally intended to cover only Oklahoma and northwest Texas; however data for 10 May 1985 were readily available and therefore included). On one of the days, the necessary conditions were met both in Oklahoma and Texas. Therefore the total number of calender days used is 34.

Morning (12 UTC) and evening (00 UTC the next day) soundings were gathered from NCAR for the day in question for all sites within 250 km of the storm(s)' FE. These soundings were supplemented by special soundings from storm-intercept projects of both NSSL and OU, and soundings from fixed NSSL sites which are operated during experiments. All these soundings were plotted and examined for errors.

A sounding representative of the environment at FE was then constructed by interpolating all soundings considered useful. The soundings included met two criteria: 1) uncontaminated by precipitation and 2) contained characteristics of air from the storm FE environment (i.e. those soundings both before and upstream from FE or those soundings both after and downstream from FE, respectively). The data were interpolated to levels every ten mb from the surface to 500 mb, and every 20 mb from 500 mb to 100 mb.

Surface maps were used to determine a surface temperature and dewpoint, representative of the time and location of FE, to which the lowest part of the sounding was adjusted. From the surface, the temperature was allowed to decrease dry-adiabatically up to the point where it intersected the temperature trace of the constructed sounding. The dewpoint temperature was allowed to decrease along a line of constant mixing ratio to meet the dewpoint trace of the constructed sounding. This was done under the assumption that the boundary layer was well mixed. Winds were subjectively interpolated and surface maps were again utilized for the lowest layers. The winds were

allowed to veer smoothly from the surface to a point where they equalled the winds of the constructed sounding (approximately 50 mb) to reflect the influences of Ekman turning and warm air advection (Davies-Jones, et. al., 1990). Heights were calculated for the new soundings using the hypsometric equation, and checks were done with neighboring soundings to make sure the constructed soundings were consistent. A total of 45 soundings were created representing 61 storms over the 34 days. Hodographs of these soundings were plotted and checked for errors.

Next, the microfilm data were reviewed and a preliminary set of modes of initial formation was determined. Evolutionary characteristics of the storms were also examined. These will be discussed in Section 3. After repeated comparisons and analyses, a final set of initial modes was defined and the storms and soundings were grouped accordingly. (Note: occasionally one sounding represents the environment of more than one storm, and these storms may be of different modes. This occurred when storms formed too closely in time and space to reasonably interpolate separate soundings for each. A sounding of this type may not be considered twice under the same mode when computing average properties of the soundings in each group.) The average time from FE to time of first severe weather report (TFSR) was computed, and student t-variable tests were performed to determine the statistical significance of the data.

Composite soundings and hodographs were developed by first converting each sounding to the following format: one level every five mb from 980 to 850 mb; one level every ten mb from 850 to 500 mb; and one level every 20 mb from 500 to 100 mb. The increased near-surface resolution was necessary to account for highly varying (from sounding to sounding) surface pressures which were originally determined as exactly as possible (not necessarily on ten mb increments). For the purpose of the composite sounding, the surface pressures were rounded to the nearest five mb and the surface elevation was changed accordingly (using the near-surface approximation that 8 meters corresponds to 1 mb) to keep the height of the 500 mb level consistent. The soundings could then be simply averaged together for thermodynamic properties and for winds (after decomposition into u and v components). It was necessary to eliminate data at the lowest few pressure levels due to the limited number of soundings with data at these levels. Therefore, the composite soundings presented in Section 3 have surface levels which vary from 960 to 945 mb.

There are certain problems inherent in several of the data sources and methods used for this study. Storm Data contains time and location errors in its severe weather reports. These errors are more numerous in the 1970's, when efforts to verify reports of severe weather were not as widespread as in recent years. The radar microfilm from the NSSL WSR-57 was of excellent quality in virtually all cases. However, the microfilm from the NWS was occasionally of poor quality. Finally, the creation of the estimated environmental soundings involved some subjectivity, as stated earlier. This implies that errors are surely present, since there is no way to know what the environment really was at FE. It is felt that smoothing inherent in the production of composite soundings will both reduce noise levels and retain any characteristic signals present in the data.

SECTION III

RESULTS

3.1 Initial Modes

The following six initial modes of formation became evident after careful review of the radar film of the 61 storms. Each definition considers only the initial stage (generally 30 minutes after FE) of the echo's development unless stated otherwise. The definition does not apply to the storm at the time of severe weather occurrence.

A). Isolated - One cell only is evident in storm formation from FE to at least 30 minutes later. No mergers are involved.

B). Pair - Two cells merge into one within 30 minutes of the second cell's FE.

C). Line segment - Three or more cells in a line merge into one cell within 30 minutes after the last cell's FE.

D). Cluster - A group of three or more cells, not arranged in a line, merge to form one cell within 30 minutes of the last cell's FE.

E). Merger - Two or more mature (VIP level 4 or greater) storms which have been in existence more than 30 minutes merge to form one storm.

F). Squall line - One initial cell becomes a part of a broken line squall line (Bluestein and Jain, 1985) which attains a length-to-width ratio greater than or equal to five and a length greater than or equal to 50 km within 30 minutes of the cell's FE.

Figure 3-1 is composed of idealized views of each of the six initial modes of formation. Generally, the left-hand third of each part (a - f) represents the outline of the radar reflectivity (at 0.5 degree elevation angle) at a time within the first 30 minutes after FE. This 30 minute period begins when the last cell to be involved directly in the final state of the thunderstorm is detected (of course, the isolated type has only one cell). The center third generally represents the storm at a time immediately after this 30 minute period, but before the storm becomes severe. (Note: none of the storms became severe in less than 30 minutes.) The right-hand third represents the storm at the time of severe weather production, also referred to as the severe stage.

Although most of these modes and their definitions are straightforward, two initial modes deserve special attention; squall line and merger. A squall-line mode storm has only one main reflectivity core throughout its first 30 minutes; in this way it is similar to an isolated-mode storm. Its inclusion in a squall line differentiates it from the isolated mode. Although the idealized storm shown remains a squall-line storm up to the time of severe weather production, this is not necessary for it to be classified as squall-line mode. Recall that only the first 30 minutes (in general) are considered when classifying the initial modes. The merger mode is the only mode involving multiple cells in which cells do not merge within the first 30 minutes of the last cell's FE. The initial cells each attain relative maturity (VIP level four), but produce no severe weather, before the storms merge. Each of the cells may have formed as any of the other five initial modes. The most important and distinctive characteristic of the merger mode is that the storms merge

after the 30 minute period following the last cell's FE.

There are a few subtle differences between certain modes that prevent them from being considered as subsets of one another. For example, the pair mode could be considered a subset of the line-segment mode. However, it was noticed that pair-mode initial cells tended to merge due to differential cell motion, while line-segment mode initial cells tended to "fill in" as they merged. One may also think that orientation is not that important, and therefore line-segment and cluster initial modes should be grouped together. However, it is felt that line-segment mode is indicative of linear forcing, while the cluster mode is indicative of areal forcing. It should be noted, though, that both tend to "fill in" as they merge.

3.2 Sounding Parameters And Other Tabulated Data

The following sounding parameters were computed. A brief summary of the importance and method of computation of each follows.

A). CAPE - Convective Available Potential Energy. CAPE, computed as in Bluestein and Jain, 1985, is directly proportional to the positive area of the skew-T log-p diagram between the level of free convection (LFC) and the equilibrium level (EL). It is given by

$$\text{CAPE} = \int_{z_1}^{z_2} g\left(\frac{\theta_c - \theta_{env}}{\theta_{env}}\right) dz \qquad (1)$$

where θ_c is the potential temperature of an air parcel having been lifted from the LFC (z_1) to the EL (z_2), and θ_{env} is the potential temperature of the unsaturated environment. CAPE is calculated using a moist adiabat through cloud base, which is assumed to be at the lifting condensation level (LCL). Both "dry" and "moist" CAPE are calculated. "Dry" CAPE, in which the actual temperature trace is used, is what is typically calculated (Bluestein and Parks, 1983, Weisman and Klemp, 1984, Bluestein and Jain, 1985). Moist CAPE is calculated using virtual temperature in place of actual temperature. This is theoretically more accurate because it takes into account the density effects of water vapor in the air. CAPE can be directly related through parcel theory to a maximum potential updraft speed, which has proven to be a good indicator of the severity of a storm. If we ignore the effects of pressure perturbation, water loading, and mixing, maximum updraft speed, w_{max}, is given by Petterssen (1956) as, $w_{max} = \sqrt{2\text{CAPE}}$.

B). LMS - Low to Mid-level Shear. This is computed as the difference in the density-weighted mean wind in the surface layer (zero to 500 m AGL) and the mean wind in the 0-to-6 km layer (Weisman and Klemp, 1982, 1984). Increasing windspeed with height is important to a storm because it aids in venting the updraft. It also provides a source of horizontal vorticity which may then be tilted into the vertical.

This measure of shear does not take into account any turning of the hodograph which may be present. However, visual inspection indicates that each of the estimated environmental soundings in this study exhibits clockwise turning of the shear vector over the lowest several kilometers. Linear theory predicts that an initially axisymmetric updraft interacts with a clockwise turning shear vector in a way that produces a dynamic vertical pressure gradient (below the level of maximum rising motion) favorable for continued rising motion on the right side of the updraft (Rotunno and Klemp, 1982). This produces preferential growth of the updraft on the right flank of the storm and

therefore produces a motion which deviates to the right of the mean wind. Computer simulations (e.g. Weisman and Klemp, 1984) have demonstrated this as well. A positive feedback mechanism can be established at this point because this deviant motion can produce further clockwise turning of the storm-relative hodograph. The importance of using storm relative hodographs has been established by several people (e.g. Maddox, 1976) and will be discussed under 3.2.E, helicity.

C). BRN - Bulk Richardson Number. This is a measure of the relative strengths of the CAPE and the LMS. It is computed here as in Weisman and Klemp, 1982, given by

$$\text{BRN} = \frac{\text{CAPE}}{1/2(\text{LMS})^2} . \qquad (2)$$

Extending the above discussion on shear, note that if a storm has both high CAPE and high shear, (including a clockwise turning of the hodograph) then the processes described above (concerning high shear) will be enhanced. As shown earlier, CAPE is directly proportional to maximum updraft strength. Therefore, a high CAPE will theoretically yield a stronger updraft which will in turn yield stronger pressure perturbations. These perturbations will then more strongly force new updraft growth on the right flank of the storm. A balance between CAPE and shear must exist for this to occur, however. BRN's in the 15 to 35 range have been shown to best represent this balance (Weisman and Klemp, 1982). Lower BRN's are indicative of relatively strong shear and/or weak buoyancy. In extreme cases, initial updrafts may be bent over by wind shear before they have time to develop into storms. Larger BRN's are indicative of weak wind shear and/or large buoyancy. In these cases, the updraft may not tilt enough to allow precipitation particles to fall out in a separate downdraft. Therefore, the updraft collapses in on itself. Long-lived updrafts are unlikely, and multicells are favored. (Note that dry and moist BRN's are calculated using dry and moist CAPE, respectively.)

D). NCAPE - Negative CAPE (also known as CIN, Convective Inhibition). This is computed similarly to CAPE, and is directly proportional to any negative area on the skew-T log-p diagram between the LCL and LFC that must be overcome to release the positive area which exists above (in height coordinates) the LFC. It is given by

$$\text{NCAPE} = -\int_{z_0}^{z_1} g\left(\frac{\theta_c - \theta_{env}}{\theta_{env}}\right) dz \qquad (3)$$

where z_0 represents the LCL and z_1 represents the LFC. Parcel theory (under the same assumptions imposed on w_{max}) provides a minimum upward velocity, w_{min}, necessary to overcome this negative area, given as, $w_{min} = \sqrt{2\text{NCAPE}}$. NCAPE is therefore also a measure of the strength of the capping inversion characteristically found just above (in height coordinates) the surface layer on many severe thunderstorm soundings (Carlson, 1982). Both dry and moist NCAPE are calculated.

E). Helicity (storm-relative). This is defined as

$$H(\boldsymbol{c}) = \int_0^h (\boldsymbol{v}-\boldsymbol{c})\cdot\boldsymbol{\omega}\ dz, \qquad (4)$$

where $\boldsymbol{v}\equiv(u(z),v(z))$ is the environmental wind from the estimated environmental

sounding, $c \equiv (c_x, c_y)$ is the storm translation velocity, and $\omega \equiv k \times dv/dz \equiv (dv/dz, du/dz)$ (Davies-Jones, et. al., 1990.) (Note: this does not include contributions from dw/dx, dw/dy, du/dy, or dv/dx). Helicity is not Galilean invariant, i.e. helicity values are reference-frame dependent. Since storms can be steady state only in their own reference frame, storm-relative helicity is the only meaningful measure of helicity. The importance of helicity has been suggested by, e.g. Lilly (1986a and b) - flows which exhibit high helicity tend not to be dissipated by turbulence as fast as flows which exhibit low helicity. Accelerating pressure gradients and helicity, both important for suppressing small-scale features within the storm, may combine with shear-induced vertical pressure gradients (see above discussion under BRN) to organize and maintain the large-scale persistent background updrafts that characterize supercells (Brandes, et. al., 1988). A physical explanation for this, following Davies-Jones, 1984, can be given by considering isentropic surfaces and vortex lines. Consider the pre-storm environment to be composed of isentropic surfaces and vortex lines which are horizontal (fig. 3-2). Because θ (potential temperature) is conserved, an initial updraft will deform the isentropic surface, forming an apparent "hill" on an otherwise horizontal (although slightly lower than before) surface. The vortex lines are not material surfaces, but due to the conservation of isentropic potential vorticity ($\Omega \cdot \nabla \theta$, where Ω is the total vorticity vector), the vortex lines remain in their original surfaces. Consider the situation in which the vorticity is purely crosswise, i.e., the mean vorticity and mean storm-relative flow are perpendicular (fig. 3-3). In this case, the maximum updraft is not collocated with either maximum in vorticity (cyclonic or anticyclonic). On the other hand, if the vorticity is purely streamwise, i.e., the mean vorticity and mean storm-relative flow are parallel, then the maximum updraft is collocated with the maximum in cyclonic vorticity (fig. 3-4) and helicity is maximized.

The helicity here is calculated in the zero-to-three km layer in ten mb increments and then multiplied by the depth of the layer. Storm motions are used both from the initial stage and the severe stage, and the 0-to-6 km mean wind is also used as a "storm motion" (to measure the helicity of a storm steered by the mean wind), in the helicity calculations (they are also used in the relative helicity and streamwise vorticity calculations - see below). Davies-Jones, Burgess, and Foster (1990) have shown that a minimum helicity value of 150 $m^2 s^{-2}$ is necessary for mesocyclone development.

F). Relative Helicity. This is defined as the helicity divided by the product of the scalar magnitudes of velocity, v, and vorticity, ω. Relative helicity is, therefore, the helicity normalized by its magnitude, and is thus dimensionless. Values are between -1.0 and 1.0, and by definition of the dot product, relative helicity is equal to the cosine of the angle between the vorticity and velocity vectors. (Note: in future works, relative helicity will be referred to as normalized helicity to have the name more closely related to the computation of the quantity.)

G). Streamwise Vorticity. This is also closely related to helicity and is equal to helicity normalized by the scalar magnitude of velocity. Streamwise vorticity is a measure of the amount of vorticity oriented along the velocity vector, and is theorized to be the origin of updraft rotation in supercells (Davies-Jones, 1984).

The other tabulated data consists of TFSR (recall that this is the time from first echo to the time of the first report of severe weather) and monthly frequency data. The TFSR was computed for each storm in the study. The month of each storm's occurrence was checked, and a bar graph was constructed showing the initial mode versus month

distributions (fig. 3-5). May had the highest frequency of storm occurrence.

Once the sounding parameters were computed, averages were obtained for each initial mode and for all soundings combined. It is important to remember that several of the 45 soundings represent the environments of more than one of the 61 storms. In cases where the storms were of different modes, the sounding was counted in each. However, a single sounding was never counted twice under the same mode, even when it represented more than one storm of that mode. This was done to ensure that each sounding in a given mode could be considered an independent data set. Averaged data for storm motions, both during the first 30 minutes of development and during a 40 minute window (+/- 20) centered on the time of the first severe weather occurrence, and TFSR data, together with the sounding parameters discussed above, are displayed in Tables 3-1a and 3-1b.

Student t-variable tests (Kenney, 1939) assuming equal variance were performed on the data in Table 3-1. A t-test tests the hypothesis that two means are different. If the average CAPE of the isolated mode is very different from the average CAPE of the other five modes combined, for example, then the t-test would find them different at a high level of confidence. Referring to Table 3-2, we see that they are different at the 79.2% level (technically, this is the p-value of the t-test). This means that out of 100 random groupings of numbers, only 21 times (approximately) would the numbers be as (or more) different as (than) in the case of our CAPE comparison. To be confident that two groups are actually different, the 95% level is typically used as the "cutoff" level. Therefore, one cannot state confidently that the average CAPE of the isolated mode storms is indeed different from the average CAPE of the rest of the storms combined.

Initially, six tests were performed: each mode separately versus the remaining five modes combined. The results from these tests are presented in Table 3-2. Afterward, 23 other carefully selected groupings of modes (isolated and pair combined versus cluster and line segment combined, for example) were tested. These results will be briefly discussed below.

Out of the six groupings shown in Table 3-2, few means were different at the 95% significance level. The CAPE (dry and moist) of the squall-line mode is low and the NCAPE (dry and moist) is high. This could be indicative of strong synoptic scale forcing, both because of the development of a continuous line of storms and because strong forcing would be necessary to overcome the large NCAPE present in the estimated environment. However, there are only two squall-line cases and generalizations cannot be made. The LMS of the cluster mode is low compared to the other five. This may have something to do with the relative lack of organization of the cluster mode. Cells simply form in proximity to one another and merge to produce the final storm. It must be remembered, however, that the shear is still strong enough to sustain a supercell (as defined here), or else the storm would not be in this study. Of course, it is possible that rapid intensification of the shear occurs between the time of the storm's FE and the time it begins to exhibit supercell characteristics.

The helicity of the pair mode (using storm motion at the time of severe weather) is significantly high. Because this is computed using the motion of the storm at the time of severe weather production and not at the time of FE, no conclusions about differences in the initial storm modes can be drawn. The only parameter for which two separate modes were found to be significantly different (when compared against the remaining five modes) was TFSR. The isolated mode has a lower TFSR (shorter time from FE to first severe report) while the pair mode has a higher TFSR. At first glance, this would seem to be easily explainable. Two cells merging into one cell would take longer to become organized than one cell remaining as one cell and therefore would take longer to produce severe weather. The situation, however, is not this simple. This will be discussed

further in the next two paragraphs.

The other 23 pairings produced relatively few significant differences. Recalling that the number of cases of each mode varies from two (squall line) to 37 (isolated), with the other four modes each having eight or fewer cases, it is not hard to understand that most of the significant differences were related to the inclusion or absence of the isolated mode in a given comparison. The listing of all results is not warranted here; however a discussion of some of the significant comparisons is in order. The direct comparison of the two modes with the most cases (isolated, 37, and line segment, eight) indicated no significant differences. The comparison of isolated modes versus pair and line-segment modes together resulted in one significant difference: the isolated-mode storms were found to average less helicity (using the initial stage motions) than the combined pair and line-segment mode storms. The comparison of line-segment mode storms against pair-mode storms produced one significant difference: the line-segment mode has a lower mean TFSR. The comparison of the isolated-mode storms against the pair-mode storms yielded one difference; the isolated mode was found to have a significantly lower TFSR. From these last two comparisons, it is seen that both isolated and line-segment modes have low TFSR, and indeed when these two modes were combined and compared to the other four modes, they yielded a significantly lower TFSR.

It is now apparent why the pair-mode TFSR versus isolated-mode TFSR situation cannot be resolved simply. The interference between the two cells in a pair-mode storm could make it slower to produce severe weather than an isolated-mode storm, all other things being equal. But, now we see that the line-segment mode also has a lower TFSR than does pair mode, even though line-segment mode storms always start with at least three initial cells. None of the other computed quantities of these three modes of storms are different at a statistically significant level. Therefore, no explanation can be derived from the data at hand.

3.3. Composite Soundings And Hodographs

The soundings were composited by pressure level. The surface pressures of individual soundings vary greatly from soundings in the Amarillo area (approximately 890 mb) to soundings from the Stephenville, TX area (approximately 970 mb), due to differences in elevation (approximately 1100 MSL in the Amarillo area vs. approximately 300 MSL in the Stephenville area). This resulted in unrealistic temperature and dewpoint traces in the lowest portion of the soundings. After careful consideration and repeated trial-and-error attempts, pressure levels that vary between 960 mb and 945 mb were chosen to be the "surfaces" for the composite soundings.

The composite soundings are presented in figure 3-6, a-g, one for each initial mode and one overall. Although the soundings appear generally similar, there are some subtle differences worth noting. The squall-line mode sounding (fig. 3-6f) has both the coolest surface temperature and the lowest surface dewpoint. These are reflected in the composite sounding statistics (Tables 3-3a and 3-3b) in the fact that the squall-line mode has the lowest CAPE. The line-segment mode sounding (fig. 3-6c) has the shallowest moist layer. The dewpoint trace begins to fall sharply at the 890 mb level. The merger-mode sounding (fig. 3-6e) has the sharpest capping inversion, with a temperature increase of two degrees C over a five mb layer, from 890 mb to 885 mb. The pair-mode sounding (fig. 3-6b) has a two-tiered capping inversion. However, this is likely due to the compositing process and is not believed to be a significant signature of the mode. None of the individual pair-mode soundings displays this characteristic. The cluster-

mode sounding (fig. 3-6d) has the lowest capping inversion (910 mb). The isolated-mode sounding (fig. 3-6a) and the overall composite sounding (fig. 3-6g) are quite similar (recall that isolated-mode storms account for 61% of the total number of storms in the study). The capping inversion, present in most of the individual soundings, has been smoothed out of these two composite soundings due to the large number of soundings composited.

The composite hodographs (fig. 3-7,a-g) are also more similar than dissimilar. However, there are some small differences which will now be summarized. The squall-line mode hodograph (fig. 3-7f) actually displays slightly more clockwise curvature in the lowest two km than any other mode. This is mainly due to a relatively weak and more veered two-km wind. It also has the highest LMS, 15.8 ms^{-1} (per six km). The line-segment mode hodograph (fig. 3-7c) has no strongly distinguishing features, and is very similar to both the isolated-mode hodograph and the overall composite (to be discussed shortly). The merger-mode hodograph (fig. 3-7e) has a pronounced low shear layer from four to five km, a feature which the pair-mode hodograph (fig. 3-7b) displays throughout the five-to-nine km layer. The cluster-mode hodograph (fig. 3-7d) is straight from the surface to two km, slowly curves to a height of four km, and then turns clockwise to a height of seven km. It has the lowest LMS, 10.5 ms^{-1}. The isolated-mode hodograph (fig. 3-7a) is curved smoothly in a clockwise sense from the surface to a height of one km, and above that it is straight. For reasons discussed above, the overall composite hodograph (fig. 3-7g) is almost identical to that of the isolated-mode hodograph.

3.4. Miscellaneous Storm Characteristics

The radar microfilm was studied from FE to at least 20 minutes after the severe stage began. During this time period several characteristics of growth were noted. These characteristics included the directional orientation of the cells of pair and line-segment initial modes, and whether or not the storm split (Wilhelmson and Klemp, 1978), backbuilt, or had a companion storm.

The orientation of the initial cells in the pair and line-segment mode storms was measured to 16 points on the compass (N, NNE, NE, ENE, etc, using standard abbreviations). These directional "bins" are 22.5 degrees wide and are centered every 22.5 degrees starting at 360 degrees. Of the six pair-mode storms, three were oriented NNE-SSW, two were NE-SW, and one was E-W (fig. 3-8a). Of the eight line-segment mode storms, one was N-S, two were NNE-SSW, four were NE-SW, and one was ENE-WSW (fig. 3-8b). Comparing the orientations to the shear vectors in the hodographs (estimated visually), it was found that in all but two of the cases (five out of six pair mode and seven out of eight line-segment mode) the orientation is along the shear vector in the one-to-one and one-half km AGL layer (fig. 3-9). This also corresponds closely to the height of cloud base (estimated by finding the LCL).

Twelve of the 61 storms in the study split (fig. 3-10). All of these were of the isolated mode. In all twelve cases the right-mover became severe and in one case the left-mover also became severe. Twenty-one of the storms exhibited backbuilding at least once. Backbuilding here is defined to occur when a relatively small cell (relative to the size of the storm) forms adjacent to and behind (considering the direction of storm motion to be forward) a storm and subsequently merges with the storm (fig. 3-11). This must occur after the time period in which the initial mode is defined (generally the first 30 minutes after FE; refer to definitions at the beginning of this chapter for more detail). One of the five cluster mode, four of the six pair mode, four of the eight line-segment mode, and 12 of the 37 isolated mode, backbuilt.

Sixteen of the 61 storms had companion storms. A companion storm is one which becomes adjacent to a storm in the study without merging with the storm (fig. 3-12). Like backbuilding, this must occur after the time period in which the initial mode is defined. Three of the five cluster mode, two of the eight line-segment mode, and 11 of the 37 isolated mode storms had companion storms. Seven of the companion storms were supercells (as defined here), seven were multicells, and two were relatively short-lived single cells (clearly not supercells).

SECTION IV

CONCLUSIONS AND DIRECTIONS OF FURTHER RESEARCH

This work was undertaken in part because 1) previous supercell case studies have generally concentrated on the severe and near-severe stages of storm evolution and have shed little light on the initial (zero to 30 minutes after FE) phases of development; and 2) computer simulations, which initialize storms with thermal "bubbles" (areas of slight temperature excess) and seem to produce what this study would define as an isolated initial mode storm (Weisman and Klemp, 1984, fig. 3), have also concentrated on the mature phases of storms, with less emphasis on the initial phase of storm development.

Therefore, this study has determined the modes of initial formation of 61 supercells that formed along or just ahead of the dryline. These modes are: isolated (37 cases); pair (six cases); line segment (eight cases); cluster (five cases); merger (three cases); and squall line (two cases). These were determined through examination of low-elevation-angle PPI scans on radar microfilm.

Data from nearby (in time and space) soundings have been used to create estimated environmental soundings for the storms. Forty-five of these soundings were created, representing the environments of the 61 storms. The soundings, and associated hodographs, were plotted and examined, and numerous sounding and hodograph parameters were computed. These data (including such parameters as CAPE, NCAPE, BRN, LMS, and storm-relative helicity) were averaged for each initial storm mode and also for all storms combined. Composite soundings were created, again for each initial mode and for all storms combined. The averaged and composite data compare favorably with earlier studies of the environments of supercell storms.

The averaged and composited data, and the composite soundings and hodographs, all indicate that the environments of the different initial modes are more alike than different. This is borne out by the fact that there are very few statistically significant differences in mode-averaged data computed from soundings and hodographs. Maddox (1976) asserted that the small-scale environment of the severe storm could not be determined through the use of environmental soundings. The findings of this research tend to lend credence to that assertion. If there are indeed differences in the environments of these six initial modes, they are small-scale and impossible to resolve with the current operational sounding network, even when supplemented by occasional "special soundings." While the implementation of a profiler network (currently underway) will increase the resolution of wind field data, thermodynamic data will remain sparse. Therefore, any small-scale features, which may play a part in differentiating between modes, will not soon be completely resolved with operational data.

Miscellaneous storm characteristics were observed. All of the storms observed to split (12) were of the isolated initial mode. This amounts to just under one-third of all isolated-mode storms (37). Twenty-one of the 61 total storms exhibited backbuilding. Sixteen of the storms had companion storms. The shear vector in the one-to-one and one-half km layer was found to be associated with the orientation of the cells in both the pair (five out of six) and line-segment (seven out of eight) mode storms.

One parameter, previously unstudied, is the time from first echo to first severe weather report (TFSR). These data indicate that the isolated and line-segment mode storms produce severe weather sooner (on average) than do the other modes. Also, pair-mode storms take longer to produce severe weather (on average) than do other modes. An overall average of 1.95 hours was determined.

As increased efforts continue in the area of mesoscale modeling, these results will be important to consider. TFSR data can be compared to the time required for model

storms to reach maturity. Also, the composite soundings and hodographs should provide a source of initialization data. Should these models be able to reproduce the initial modes given here, a dynamical determination of the differences in the initial modes will be possible (due to the high-resolution data produced in numerical models), as opposed to the observational determinations made in this study.

It is believed that this study will be of some benefit to nowcasters in operational meteorology, specifically in the Southern Plains. By observing the initial mode of development of dryline storms, an educated guess can now be made as to how long the storms will develop before severe weather will be produced. The standard deviations of the TFSR calculations are large, however, and these findings should be used only as guidelines in prediction.

Future mesoscale modeling efforts should address the area of initial development. Investigation of storm development in the models, with varying numbers of thermal "bubbles", could prove valuable. Altering the orientation of the thermals, particularly with respect to the shear vector at cloud base, could aid in understanding why they seem to be related, as noted observationally in this study. Hopefully, computer simulations will progress to the point where thermals will not be needed to initiate storms. Then, perhaps, these modes can be more realistically modelled.

BIBLIOGRAPHY

Beebe, R. G., 1958: Tornado proximity soundings. Bull. Amer. Meteor. Soc., 39, 195-201.

Blanchard, D. O., 1990: Mesoscale convective patterns of the Southern High Plains. Bull. Amer. Meteor. Soc., 71, 994-1005.

Bluestein, H. B., 1983: Surface meteorological observations in severe thunderstorms. Part II: Field experiments with TOTO. J. Clim. Appl. Meteor., 22, 919-930.

_____, and M. H. Jain, 1985: Formation of mesoscale lines of precipitation: Severe squall lines in Oklahoma during the Spring. J. Atmos. Sci., 42, 1711-1732.

_____, and C. R. Parks, 1983: A synoptic and photographic climatology of low-precipitation severe thunderstorms in the Southern Plains. Mon. Wea. Rev., 111, 2034-2046.

_____, G. T. Marx, and M. H. Jain, 1987: Formation of mesoscale lines of precipitation: Nonsevere squall lines in Oklahoma during the spring. J. Atmos. Sci., 42, 1711-1732.

Brandes, E. A., R. P. Davies-Jones, and B. C. Johnson, 1988: Streamwise vorticity effects on supercell morphology and persistence. J. Atmos. Sci., 45, 947-963.

Browning, K. A., 1964: Airflow and precipitation trajectories within severe local storms which travel to the right of the mean winds. J. Atmos. Sci., 21, 634-639.

_____, 1968: The organization of severe local storms. Weather, 23, 429-434.

Carlson, T. N.,1982: The role of the lid in severe storm formation: Some synoptic examples from SESAME. Preprints, 12th Conf. on Severe Local Storms, Amer.Meteor. Soc., 221-224.

_____, and F. H. Ludlum, 1968: Conditions for the formation of severe local storms. Tellus, 20, 203-226.

Darkow, G. L., 1969: An analysis of over sixty tornado proximity soundings. Preprints, 6th Conf. on Severe Local Storms, Amer. Meteor. Soc., 218-221.

Davies-Jones, R. P., 1984: Streamwise vorticity: The origin of updraft rotation in supercell storms. J. Atmos. Sci., 41, 2991-3006.

_____, and D. Zacharias, 1988: Contributing factors in the 10 May 1985 tornado outbreak in northwest Kansas. Preprints, 15th Conf. on Severe Local Storms, Amer. Meteor. Soc., 284-287.

_____, _____, and Michael P. Foster, 1990: Test of helicity as a tornado forecast parameter. Preprints, 16th Conf. on Severe Local Storms, Amer. Meteor. Soc.

Fawbush, E. J., and R. C. Miller, 1952: A mean sounding representative of the tornadic airmass environment. Bull. Amer. Meteor. Soc., 33, 303-307.

Foote, G. B., and H. W. Frank, 1983: Case study of a hailstorm in Colorado. Part III: Airflows from triple-Doppler measurements. J. Atmos. Sci., 40, 686-707.

Fujita, T. T., 1958: Structure and movement of a dry front. Bull. Amer. Meteor. Soc., 32, 1-9.

Golden, J. H., 1980: Forecasting and research on severe storms in China: A summary of two seminars. Bull. Amer. Meteor. Soc., 61, 7-21.

Houze, R. A., B. F. Smull, and P. Dodge, 1990: Mesoscale organization of springtime rainstorms in Oklahoma. Mon. Wea. Rev., 118, 613-654.

Kenney, J. F., 1939: Mathematics of Statistics, Pt. 1. D. Van Nostrand Co., New York. p. 140-141

Klemp, J. B., 1987: Dynamics of tornadic thunderstorms. Ann. Rev. Fluid Mech., 19, 369-402.

_____, and R. Rotunno, 1983: A study of the tornadic region within a supercell thunderstorm. J. Atmos. Sci., 40, 359-377.

Lemon, L. R., and C. A. Doswell, 1979: Severe thunderstorm evolution and mesocyclone structure as related to tornadogenesis. Mon. Wea. Rev., 107, 1184-1197.

_____, 1977: New severe thunderstorm radar identification techniques and warning criteria: A preliminary report. NOAA Tech. Memo. NWS-NSSFC 1, 60 pp. [NTIS No. PB-273049.]

Lilly, D. K., 1986a: The structure, energetics and propagation of rotating storms. Part I: Energy exchange with the mean flow. J. Atmos. Sci., 43, 113-125.

_____, 1986b: The structure, energetics and propagation of rotating storms. Part II: Helicity and storm stabilization. J. Atmos. Sci., 43, 126-140.

_____, and T. Gal-Chen, 1990: Can dryline mixing create buoyancy? J. Atmos. Sci., 47, 1170-1171.

Maddox, R. A., 1976: An evaluation of tornado proximity wind and stability data. Mon. Wea. Rev., 104, 133-142.

McCarthy, J., and S. E. Koch, 1982: The evolution of an Oklahoma dryline. Part I: A meso- and subsynoptic-scale analysis. J. Atmos. Sci., 39, 225-236.

McGinley, J. A. and Y. Sasaki, 1975: The role of symmetric instability in thunderstorm development on the dryline. Preprints, 9th Conf. on Severe Local Storms, Omaha, 173-180.

Miller, M. J., and R. Pearce, 1974: A three-dimensional primitive equation model of cumulus convection. Quart. J. Roy. Meteor. Soc., 100, 133-154.

Petterssen, S., 1956: Weather Forecasting and Analysis. Vol II, second edition. McGraw-Hill, New York. p. 136.

Rhea, J. O., 1966: A study of thunderstorm formation along dry lines. J. Appl. Meteor., 5, 58-63.

Rotunno, R., and J. B. Klemp, 1982: The influence of the shear-induced pressure gradient on thunderstorm motion. Mon. Wea. Rev., 110, 136-151.

_____, and _____, 1985: On the rotation and propagation of simulated supercell thunderstorms. J. Atmos. Sci., 42, 271-292.

Schaefer, J. T., 1974a: A simulative model of dryline motion. J. Atmos. Sci., 31, 956-964.

_____, 1974b: The life cycle of the dryline. J. Appl. Meteor., 13, 444-449.

_____, 1975: Nonlinear biconstituent diffusion: a possible trigger mechanism of convection. J. Atmos. Sci., 32, 2278-2284.

Schlesinger, R. E., 1978: A three-dimensional numerical model of an isolated thunderstorm. Part I: Comparative experiments for variable ambient shear. J. Atmos. Sci., 35, 690-713.

Tegtmeier, S. A., 1974: The role of the surface, sub-synoptic, low pressure system in severe weather forecasting. M. S. Thesis, School of Meteorology, University of Oklahoma, 66 pp.

Vasiloff, S. V., E. A. Brandes, and R. P. Davies-Jones, 1986: An investigation of the transition from multicell to supercell storms. J. Clim. Appl. Meteor., 25, 1022-1036.

Weisman, M. L., and J. B. Klemp, 1982: The dependence of numerically simulated convective storms on vertical wind shear and buoyancy. Mon. Wea. Rev., 110, 504-520.

_____, and _____, 1984: The structure and classification of numerically simulated convective storms in directionally varying wind shears. Mon. Wea. Rev., 112, 2479-2498.

Weston, K. J., 1972: The dry-line of Northern India and its role in cumulonimbus convection. Quart. J. R. Met. Soc., 98, 519-531.

Wilhelmson, R. B., 1974: The life cycle of a thunderstorm in three dimensions. J. Atmos. Sci., 31, 1629-1651.

Wilhelmson, R.B., and J. B. Klemp, 1978: A numerical study of storm splitting that leads to long-lived storms. J. Atmos. Sci., 35, 1974-1986.

Wills, T. G., 1969: Characteristics of the tornado environment as deduced from proximity soundings. Preprints, 8th Conf. on Severe Local Storms, Amer. Meteor. Soc., 222-228.

APPENDIX A

TORNADIC VS. NONTORNADIC COMPARISON

As a final step in this research, storms were grouped by whether or not they produced tornadoes at some time (not necessarily the first report of severe weather). Data from the individual soundings representing the environments of the storms were averaged and appear in Tables A-1 and A-2. None of the differences between averaged tornadic and nontornadic data are statistically significant at the 95% confidence level. Therefore, no conclusions should be drawn concerning apparent differences.

The soundings were composited as before, only this time by tornadic vs. nontornadic storms. The main difference in the two soundings is that the nontornadic storm composite (fig. A-2) retains a capping inversion near 900 mb, whereas in the tornadic composite sounding (fig. A-1), the inversion has been smoothed away. As discussed in the main text, it is believed that when many soundings are composited together, features such as the capping inversion are lost due to smoothing. Therefore, the difference in the capping inversion is not believed to be meteorologically significant. The main difference in the hodographs is in the three-to-seven km layer. The tornadic composite (fig. A-3) has a slight clockwise curvature in this layer while the nontornadic composite (fig. A-4) is straight. One other difference is in the maximum windspeed in the hodograph. The nontornadic composite hodograph (fig. A-4) has a larger ten km windspeed than the tornadic composite hodograph (fig. A-3).

Data derived from the composite sounding and hodograph are presented in Tables A-3 and A-4, respectively. They are similar to the averaged data with the following exceptions. The BRNs of the nontornadic storms are much lower for the composited sounding than for the averaged data. The relative helicity values for both tornadic and nontornadic storms are considerably higher in the composite data for initial and severe storm motions than in the averaged data.

Table A-5 lists the number of tornadic and nontornadic storms by initial mode, while Table A-6 lists them by characteristics of evolution. Recalling that all storms that experienced splitting are of the isolated mode (Section 3.4), we note that while more than half of the isolated-mode storms were tornadic, only three of twelve isolated-mode storms that split became tornadic. In fact, excluding those isolated-mode storms which split, more than two-third of the isolated-mode storms remaining became tornadic. The results indicate that storms that split are less likely to produce tornadoes than storms that do not. This should be especially important for warning meteorologists to bear in mind.

Type Number of Storms / Number of Soundings	CAPE		NCAPE		BRN		LMS	TFSR
	Dry	Moist	Dry	Moist	Dry	Moist		
Isolated 37 / 29	3116 (861)	2662 (802)	28.2 (30.8)	17.1 (22.2)	35 (20)	30 (18)	15 (3.3)	1.77 (0.83)
Pair 6 / 6	3201 (1123)	2780 (1029)	17.8 (10.1)	3.3 (2.2)	29 (13)	25 (12)	16 (3.7)	2.69 (0.88)
Line Segment 8 / 7	2926 (1014)	2484 (1006)	32.7 (65.7)	38.9 (71.4)	39 (23)	34 (21)	14 (4.3)	1.76 (0.38)
Cluster 5 / 4	2903 (804)	2266 (909)	64.5 (61.6)	55.9 (48.4)	54 (33)	43 (33)	11 (1.8)	2.19 (0.86)
Merger 3 / 3	2674 (506)	2255 (503)	14.6 (12.5)	16.0 (15.2)	35 (26)	31 (24)	15 (6.2)	2.66 (1.50)
Squall Line 2 / 2	1403 (26)	998 (69)	140.0 (87.8)	119.0 (97.6)	11 (0)	8 (1)	16 (0)	2.13 (0.29)
Overall 61 / 45	3032 (960)	2531 (877)	34.4 (46.6)	27.4 (43.7)	36 (22)	30 (19)	14 (3.8)	1.95 (0.86)

Table 3-1a. Averaged computed parameters from soundings, and TFSR data. Units: CAPE, NCAPE in J kg^{-1}; BRN is dimensionless; LMS in ms^{-1} (see Appendix A for method of computation); TFSR in hours. The numbers in parentheses are standard deviations. Directly under the storm mode name are: left box, number of different storms of that given mode in the study; right box, number of different soundings of that given mode contributing data to the averages.

Mode	Number of Storms	Number of Soundings	Indicated Motion Type	Dir. from	Speed	Relative Helicity	Helicity	Streamwise Vorticity
Isolated	37	29	0 - 6 km	223°	17.9	.2214 (.2913)	112.2 (111.1)	.0031 (.0033)
			Initial	221°	12.3	.3840 (.3071)	128.6 (110.8)	.0045 (.0034)
			Severe	235°	9.2	.4854 (.2391)	211.5 (181.5)	.0054 (.0033)
Pair	6	6	0 - 6 km	222°	20.6	.2924 (.3127)	100.6 (87.1)	.0042 (.0025)
			Initial	220°	10.8	.4544 (.2586)	207.7 (116.1)	.0055 (.0028)
			Severe	256°	10.6	.6172 (.1414)	352.1 (116.4)	.0073 (.0013)
Line Segment	8	7	0 - 6 km	220°	19.4	.2418 (.3163)	129.3 (66.2)	.0045 (.0027)
			Initial	223°	12.7	.2876 (.2752)	204.1 (113.1)	.0052 (.0033)
			Severe	236°	10.4	.4617 (.2226)	227.7 (86.3)	.0061 (.0022)
Cluster	5	4	0 - 6 km	222°	15.4	.2118 (.2064)	48.6 (27.6)	.0022 (.0014)
			Initial	257°	5.8	.3580 (.2526)	98.9 (63.6)	.0031 (.0019)
			Severe	247°	7.4	.4895 (.1927)	155.7 (58.8)	.0050 (.0010)
Merger	3	3	0 - 6 km	219°	19.8	.1464 (.4199)	64.6 (53.7)	.0032 (.0018)
			Initial	220°	13.4	.2936 (.3802)	83.4 (26.3)	.0037 (.0029)
			Severe	230°	10.5	.3847 (.0677)	141.1 (25.1)	.0048 (.0011)
Squall Line	2	2	0 - 6 km	234°	19.1	.2825 (.3337)	162.6 (61.9)	.0037 (.0034)
			Initial	240°	12.8	.4714 (.5411)	323.7 (—)	.0055 (.0057)
			Severe	266°	13.7	.5119 (.0475)	373.1 (21.0)	.0075 (.0001)
Overall	61	45	0 - 6 km	221°	18.1	.2298 (.2867)	107.4 (96.1)	.0033 (.0030)
			Initial	222°	11.9	.3775 (.2917)	146.3 (113.7)	.0046 (.0032)
			Severe	238°	11.1	.4915 (.2161)	221.4 (158.7)	.0057 (.0028)

Table 3-1b. As in Table 3-1a, but from hodographs. Units are: relative helicity, dimensionless; helicity, m^2s^{-2}; streamwise vorticity, s^{-1}; speed, ms^{-1}. The indicated motions are as follows: 0-6 km, 0-6 km mean wind; initial, motion of the storm during the first 30 minutes after FE; severe, motion of the storm during the 40 minute period centered (+/- 20 minutes) on the time of the first severe weather occurrence.

Table 3-2. Statistical significances. See caption next page.

	Isolated (37) vs Other (24)		Pair (6) vs Other (55)		Line Seg (8) vs Other (53)		Cluster (5) vs Other (56)		Merger (3) vs Other (58)		Squall Line (2) vs Other (59)	
Dry CAPE	29	22	6	45	7	44	4	47	3	48	2	49
	N	79.2	N	47.4	N	11.5	N	47.1	N	43.3	Y	98.7
Moist CAPE	29	22	6	45	7	44	4	47	3	48	2	49
	N	77.6	N	53.5	N	12.1	N	46.6	N	42.1	Y	99.0
LMS	29	22	6	45	7	44	4	47	3	48	2	49
	N	28.0	N	70.0	N	40.4	Y	95.2	N	23.4	N	47.6
BRN	29	22	6	45	7	44	4	47	3	48	2	49
	N	0.9	N	56.8	N	39.5	N	85.9	N	0.3	N	89.7
Moist BRN	29	22	6	45	7	44	4	47	3	48	2	49
	N	1.9	N	51.3	N	37.8	N	84.9	N	3.3	N	90.3
Dry NCAPE	26	20	4	42	7	39	4	42	3	43	2	44
	N	74.1	N	55.6	N	11.6	N	80.8	N	56.2	Y	99.9
Moist NCAPE	19	15	4	30	4	30	3	31	2	32	2	32
	N	87.6	N	75.4	N	41.7	N	75.7	N	29.1	Y	99.9
Month	37	24	6	55	8	53	5	56	3	58	2	59
	N	65.0	N	60.3	N	47.2	N	43.0	N	20.7	N	89.0
TFSR	37	24	6	55	8	53	5	56	3	58	2	59
	Y	96.7	Y	97.7	N	46.1	N	50.3	N	86.4	N	24.4
Mean Relative Helicity	29	22	6	45	7	44	4	47	3	48	2	49
	N	18.7	N	42.6	N	9.4	N	10.2	N	39.1	N	20.6
Initial Relative Helicity	35	18	5	48	7	46	3	50	2	51	1	52
	N	18.3	N	64.7	N	58.9	N	51.4	N	81.2	N	87.1
Severe Relative Helicity	36	24	6	54	8	52	5	55	3	57	2	58
	N	11.0	N	85.3	N	37.0	N	5.7	N	63.9	N	8.3
Mean Helicity	29	22	6	45	7	44	4	47	3	48	2	49
	N	31.9	N	14.5	N	48.3	N	79.9	N	57.3	N	59.3
Initial Helicity	35	18	5	48	7	46	3	50	2	51	1	52
	N	89.0	N	79.7	N	85.4	N	54.3	N	57.6	N	88.8
Severe Helicity	36	24	6	54	8	52	5	55	3	57	2	58
	N	57.5	Y	96.3	N	4.2	N	68.8	N	64.8	N	81.9
Mean Streamwise Vorticity	29	22	6	45	7	44	4	47	3	48	2	49
	N	39.3	N	54.9	N	42.2	N	55.1	N	4.5	N	15.3
Initial Streamwise Vorticity	35	18	5	48	7	46	3	50	2	51	1	52
	N	81.7	N	78.7	N	59.8	N	25.1	N	59.6	N	88.8
Severe Streamwise Helicity	36	24	6	54	8	52	5	55	3	57	2	58
	N	62.2	N	84.9	N	29.4	N	44.7	N	43.2	N	64.0

Table 3-2. Statistical significance test results, testing the means of averaged computed sounding parameters (and other computed data) of each mode of storm vs. the other five modes combined. Each square contains 4 numbers or letters. These are: top left, number of soundings used for the mode indicated at the top of that column; top right, as in the top left, but for the soundings of the remaining five modes of storms; bottom left, "yes" or "no" answering the following question,"Are the means different at or above the 95% confidence level?"; bottom right, percentage chance that the means are statistically different. Numbers in parentheses are total number of storms of the indicated groups. "Mean", "Initial", and "Severe", as adjectives to the computed parameters reflect the use of 0-6 km mean wind, initial stage storm motion, and severe stage storm motion, respectively, in the computations of the indicated parameters.

Mode	Number of Storms	Number of Soundings	CAPE Dry	CAPE Moist	NCAPE Dry	NCAPE Moist	BRN Dry	BRN Moist	LMS
Isolated	37	29	2853	2408	26.0	5.8	35	30	13
Pair	6	6	2733	2294	32.3	13.3	29	25	14
Line Segment	8	7	2771	2279	89.3	57.0	44	36	11
Cluster	5	4	2125	1704	104.2	76.0	38	31	11
Merger	3	3	2661	2180	90.8	76.3	24	20	15
Squall Line	2	2	1391	987	137.2	113.8	11	8	16
Overall	61	45	2708	2255	42.5	18.7	36	30	12

Table 3-3a. As in Table 3-1a, but for data from composite soundings.

Mode	Number of Storms	Number of Soundings	Indicated Motion Type	Dir. from	Speed	Relative Helicity	Helictiy	Streamwise Vorticity
Isolated	37	29	0 - 6 km	223°	17.9	.2812	63.6	.0021
			Initial	221°	12.3	.7841	105.6	.0052
			Severe	235°	9.2	.8798	150.9	.0056
Pair	6	6	0 - 6 km	222°	20.6	.4547	36.9	.0027
			Initial	220°	10.8	.7536	126.0	.0052
			Severe	256°	10.6	.8851	251.7	.0062
Line Segment	8	7	0 - 6 km	220°	19.4	-.1324	56.7	.0006
			Initial	223°	12.7	.6790	111.9	.0053
			Severe	236°	10.4	.7596	164.7	.0058
Cluster	5	4	0 - 6 km	222°	15.4	.4447	39.0	.0024
			Initial	257°	5.8	.6835	86.1	.0041
			Severe	247°	7.4	.7971	125.1	.0047
Merger	3	3	0 - 6 km	219°	19.8	.2101	54.3	.0017
			Initial	220°	13.4	.5560	90.3	.0046
			Severe	230°	10.5	.6782	139.5	.0057
Squall Line	2	2	0 - 6 km	234°	19.1	-.0654	144.6	.0017
			Initial	240°	12.8	.6022	225.9	.0076
			Severe	266°	13.7	.7048	353.4	.0080
Overall	61	45	0 - 6 km	221°	18.1	.2671	59.1	.0020
			Initial	222°	11.9	.8136	105.9	.0052
			Severe	238°	11.1	.9129	161.1	.0057

Table 3-3b. As in Table 3-1b, but for data from composite hodographs. Indicated motions are from averaged data.

Type		CAPE		NCAPE		BRN			
Number of Storms	Number of Soundings	Dry	Moist	Dry	Moist	Dry	Moist	LMS	TFSR
Tornadic	36 31	3198 (1026)	2737 (967)	31.4 (45.7)	27.0 (45.0)	37 (21)	32 (20)	14.0 (3.6)	1.8.4 (0.84)
Non-tornadic	25 22	2882 (789)	2464 (770)	35.3 (44.0)	21.5 (38.0)	38 (25)	32 (23)	13.9 (5.3)	2.11 (0.87)

Table A-1. As in Table 3-1a, but for tornadic vs. nontornadic storms.

Type		Indicated Motion			Relative Helicity	Helicity	Streamwise Vorticity
Number of Storms	Number of Soundings	Type	Dir. from	Speed			
Tornadic	36 31	0 - 6 km	221°	19.2	.2542 (.2455)	105.6 (91.6)	.0030 (.0028)
		Initial	221°	12.5	.3874 (.3113)	146.2 (107.6)	.0047 (.0031)
		Severe	239°	10.8	.5161 (.1695)	230.5 (146.5)	.0059 (.0023)
Non-tornadic	25 22	0 - 6 km	223°	16.8	.2288 (.3365)	126.3 (125.3)	.0037 (.0038)
		Initial	223°	11.1	.3560 (.2763)	152.6 (145.1)	.0045 (.0038)
		Severe	237°	11.7	.4586 (.2710)	208.5 (178.6)	.0053 (.0033)

Table A-2. As in Table 3-1b, but for tornadic vs. nontornadic storms.

Type		CAPE		NCAPE		BRN		
Number of Storms	Number of Soundings	Dry	Moist	Dry	Moist	Dry	Moist	LMS
Tornadic	36 31	2982	2505	33	13	37	31	13
Non-tornadic	25 22	2429	1985	77	47	32	26	12

Table A-3. As in Table A-1, but for composite soundings.

Type		Indicated Motion			Relative Helicity	Helicity	Streamwise Vorticity
Number of Storms	Number of Soundings	Type	Dir. from	Speed			
Tornadic	36 31	0 - 6 km	221°	19.2	.3199	74.1	.0023
		Initial	221°	12.5	.7861	115.2	.0055
		Severe	239°	10.8	.9014	183.0	.0061
Non-tornadic	25 22	0 - 6 km	223°	16.8	.1391	71.1	.0018
		Initial	223°	11.1	.7934	112.5	.0055
		Severe	237°	11.7	.8316	150.9	.0057

Table A-4. As in Table A-2, but for composite hodographs.

Mode	Tornadic	Non-tornadic
Isolated	21	16
Pair	4	2
Line Segment	5	3
Cluster	2	3
Merger	2	1
Squall Line	2	0

Table A-5. Tornadic vs. nontornadic storms by initial mode. Greater than half of the storms in all modes other than cluster mode produced tornadoes.

Characteristic	Tornadic	Non-tornadic
Companion	11	5
Splitting	3	9
Backbuilding	13	8

Table A-6. Characteristics of evolution for tornadic vs. nontornadic storms. The number of storms experiencing splitting, backbuilding, or companion storms are listed.

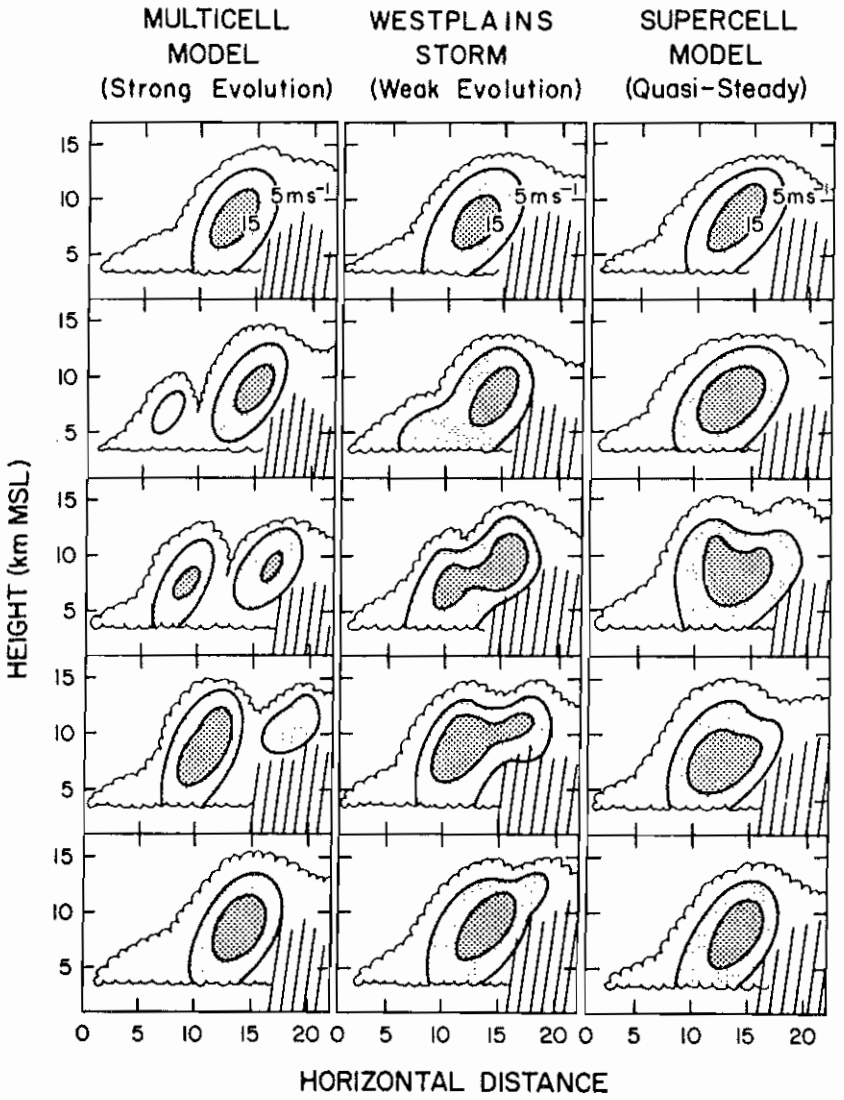

Fig. 1-1. Schematic diagram showing updraft evolution for three different storm models. The contours represent isotachs of vertical wind speed. The left panel depicts the cellular evolution according to the multicell model, involving the formation of discrete updrafts. In the supercell model, on the right, the updraft is shown as being quasi-steady. In the model deduced for the WestPlains storm, shown in the middle, the large updraft undergoes gradual changes but remains singly connected. This is termed weak evolution, in contrast to the strong evolution of the multicell case. The time between successive frames, moving down the figure, is meant to be 3-5 minutes. (from Foote and Frank, 1983).

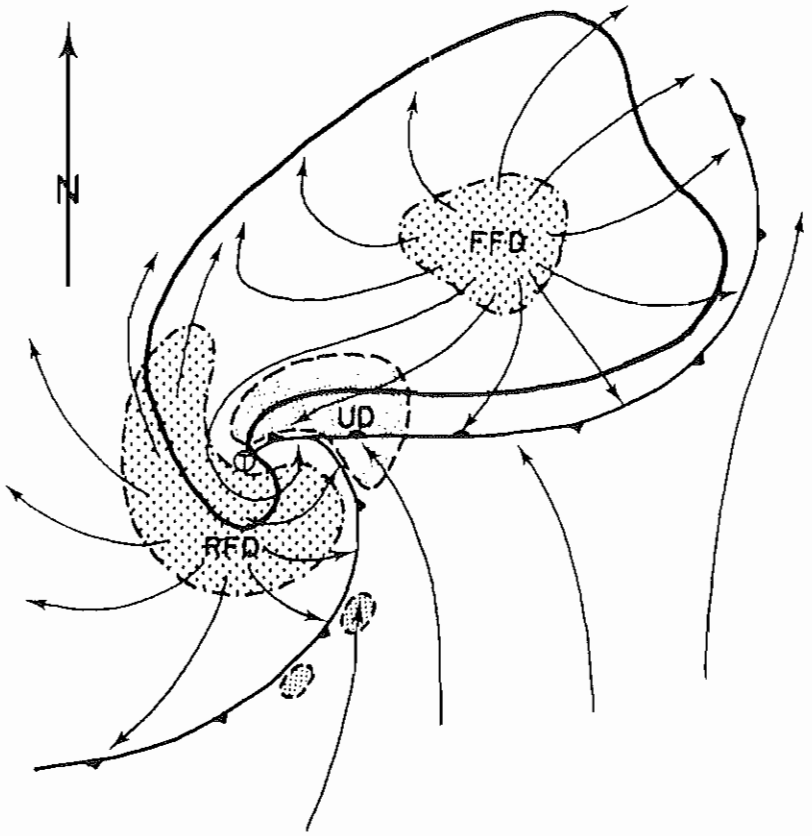

Fig. 1-2. Schematic plan view of a tornadic thunderstorm (supercell) at the surface. Thick line encompasses radar echo. The thunderstorm "gust front" structure and "occluded" wave are also depicted using a solid line and frontal symbols. Surface positions of the updraft (UD) are finely stippled, forward flank downdraft (FFD) and rear flank downdraft (RFD) are coarsely stippled, and associated streamlines (relative to the ground) are also shown. Tornado location is shown by an encircled T. (from Lemon and Doswell, 1979).

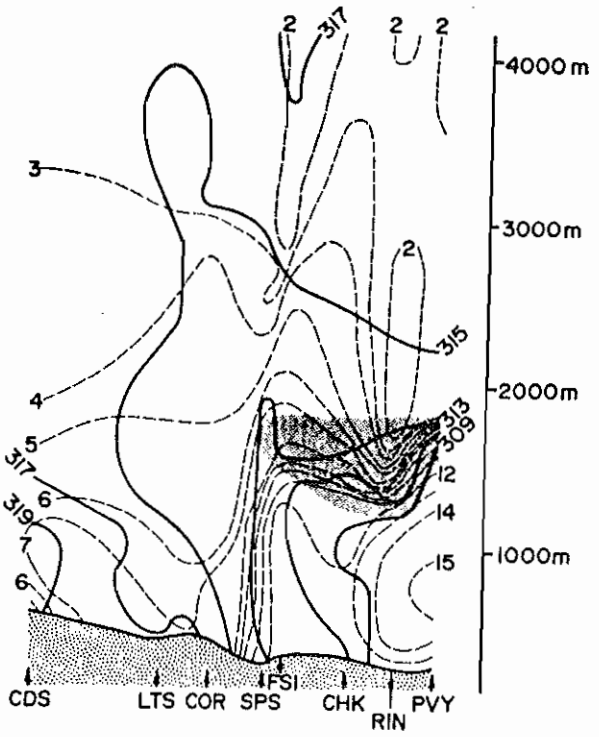

Fig. 1-3. Example of dryline vertical structure from 1400 CST (2000 UTC) 22 May 1966, from Childress, Texas (CDS) to Pauls Valley, Oklahoma (PVS). Dark lines are potential temperature in degrees K while dashed lines are mixing ratio in gm kg^{-1}. Shading denotes low-level inversion or markedly stable layer. (from Schaefer, 1974b).

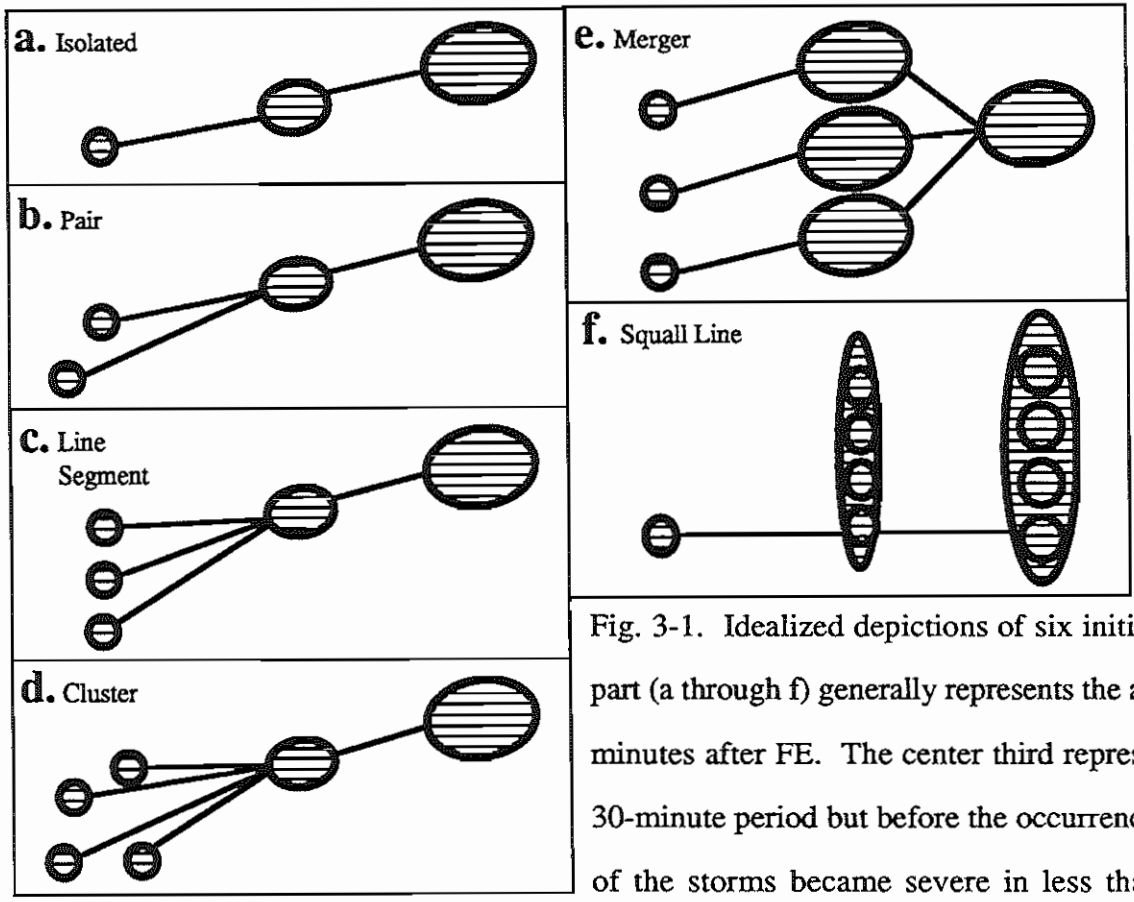

Fig. 3-1. Idealized depictions of six initial modes. The left third of each part (a through f) generally represents the appearance of the storm within 30 minutes after FE. The center third represents storm appearance after this 30-minute period but before the occurrence of severe weather. Note: none of the storms became severe in less than 30 minutes. The right third represents storm appearance at the time of severe weather production. see text for further details.

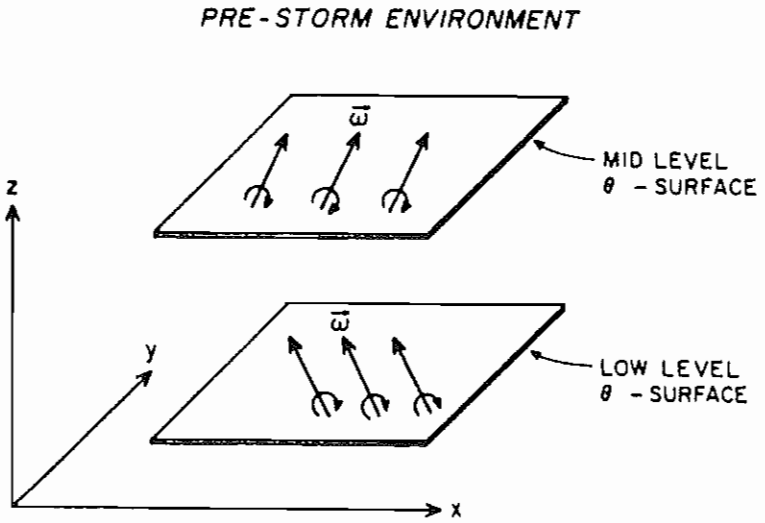

Fig. 3-2. Isentropic surfaces and vorticity vectors in the pre-storm environment. (from Davies-Jones, 1984).

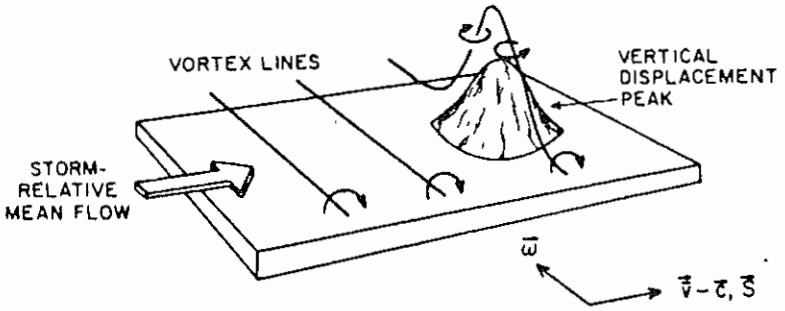

Fig. 3-3. Effect of localized vertical displacement "hill" on vortex lines when mean vorticity, ω, and mean storm-relative flow, $\bar{v}$-c, are perpendicular (purely crosswise vorticity). (from Davies-Jones, 1984).

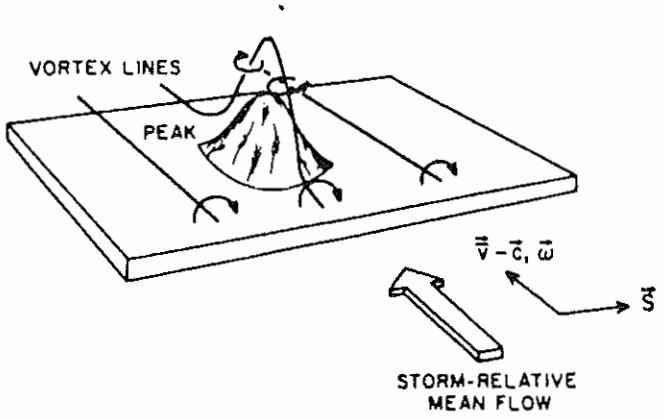

Fig. 3-4. As in fig. 3-3, but for the case when the vorticity is purely streamwise, i.e. mean vorticity, ω, and mean storm-relative flow, $\bar{v}$-c, are parallel. (from Davies-Jones, 1984).

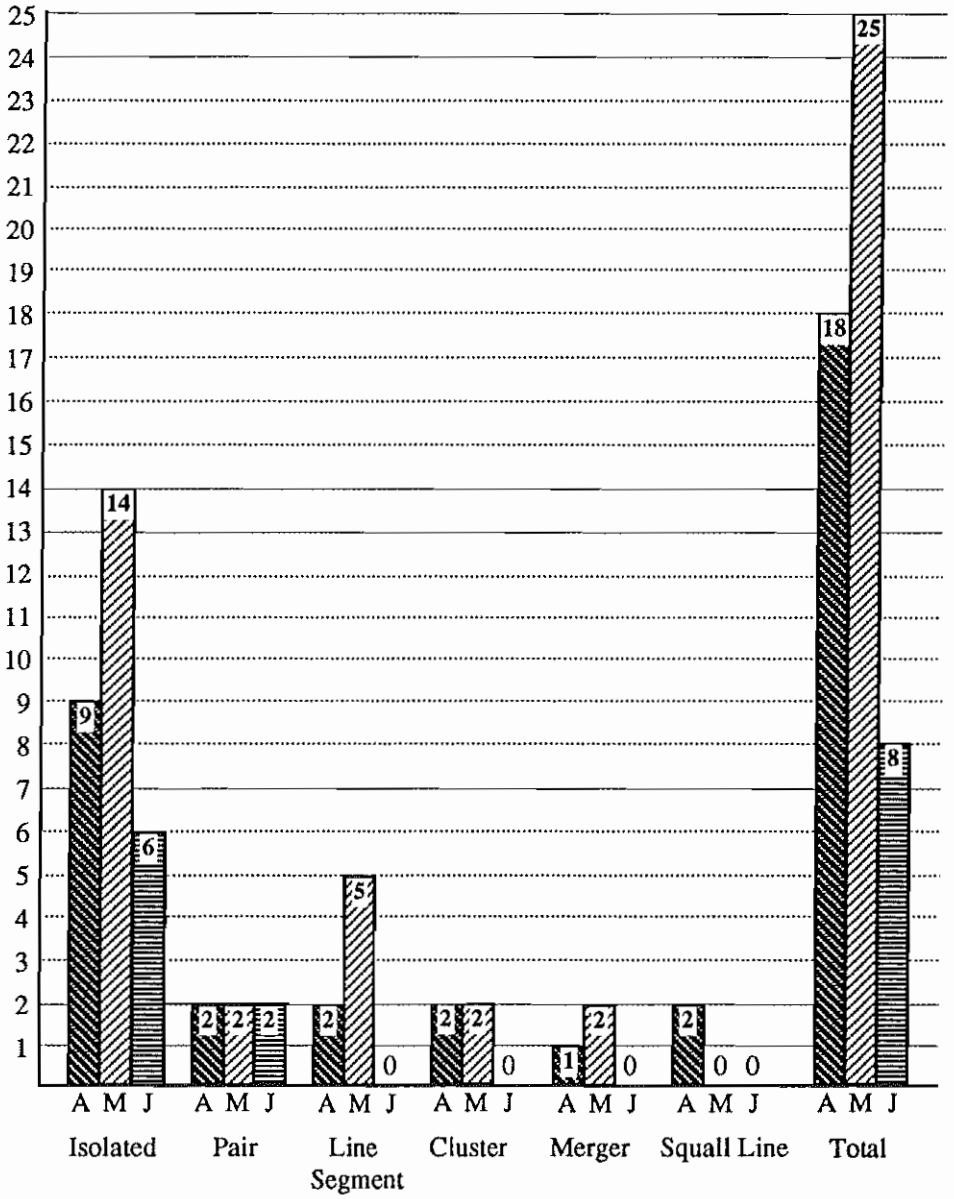

Fig. 3-5. Number of soundings used to create composite soundings by month and storm mode. "A" corresponds to April, "M" to May, and "J" to June. The total does not equal 45 (the total number of separate soundings) because some soundings are used more than once. This occurs when storms of different modes are represented by a single sounding. There were six such soundings.

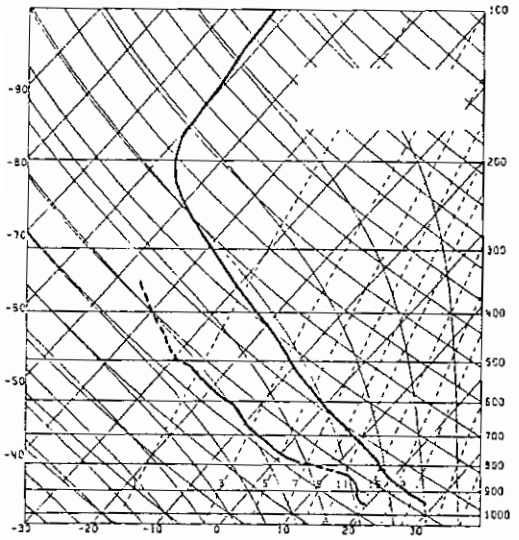

Fig. 3-6a. Sounding for isolated-mode composite.

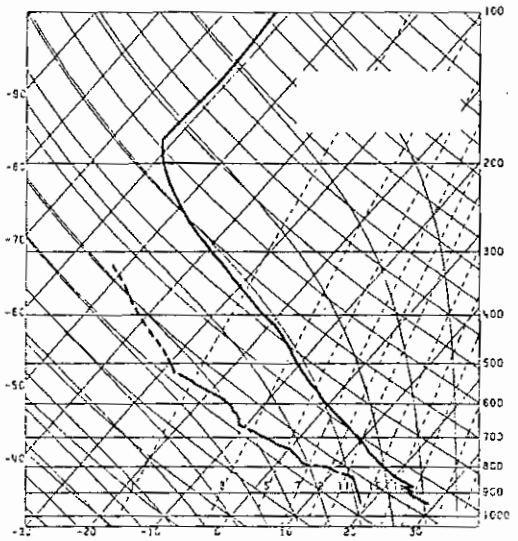

Fig. 3-6b. Sounding for pair-mode composite.

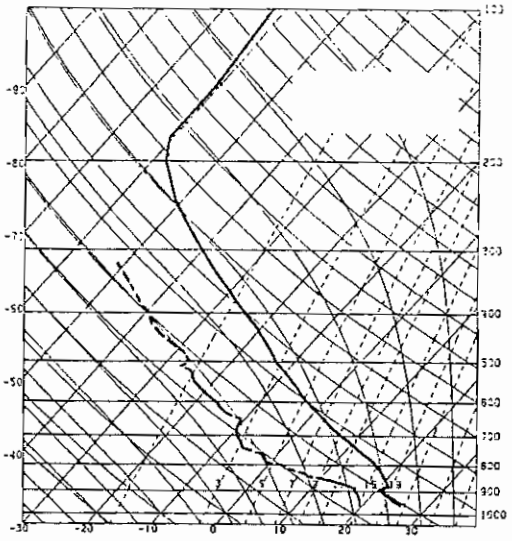

Fig. 3-6c. Sounding for line-segment mode composite.

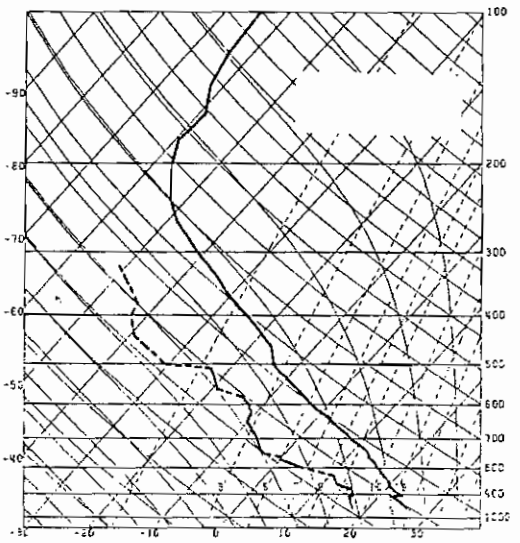

Fig. 3-6d. Sounding for cluster mode composite.

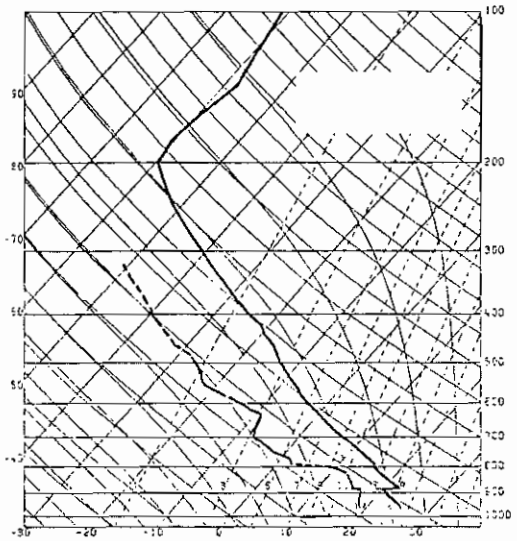

Fig. 3-6e. Sounding for merger mode composite.

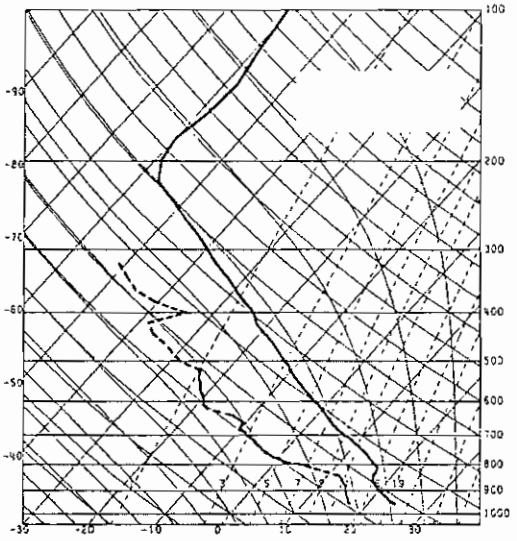

Fig. 3-6f. Sounding for squall-line mode composite.

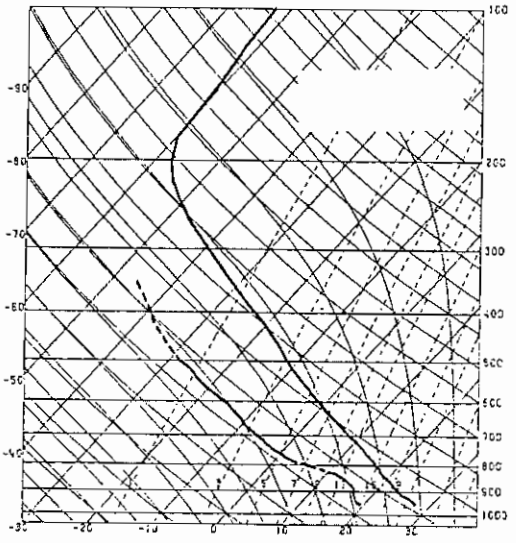

Fig. 3-6g. Overall composite sounding.

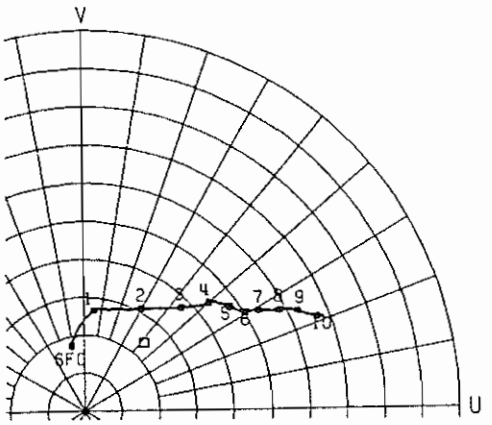

Fig. 3-7a. Hodograph for isolated-mode composite.

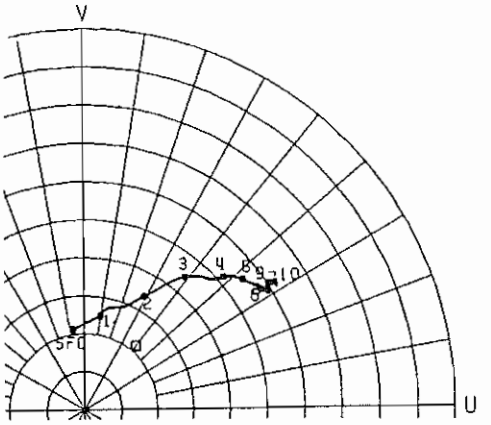

Fig. 3-7b. Hodograph for pair-mode composite.

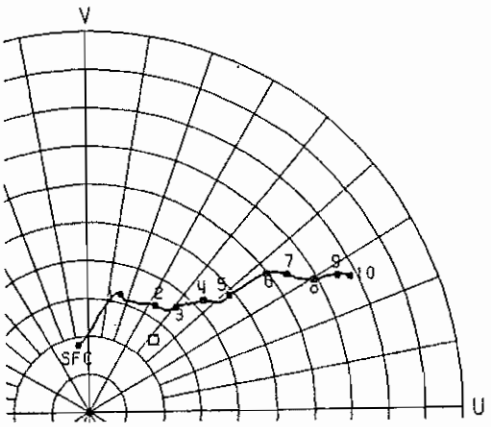

Fig. 3-7c. Hodograph for line-segment mode composite.

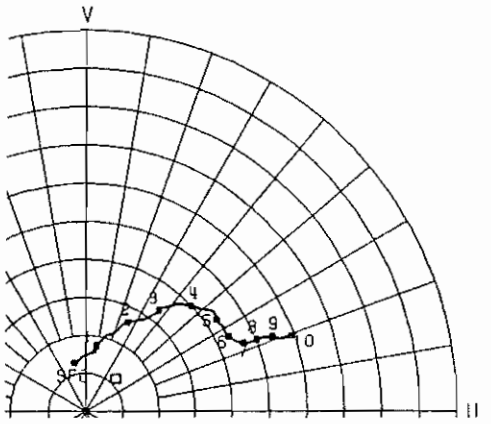

Fig. 3-7d. Hodograph for cluster-mode composite.

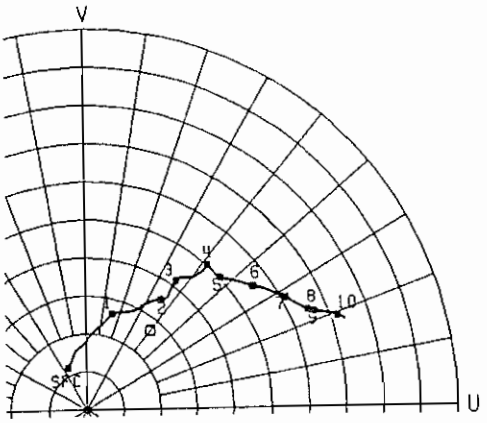

Fig. 3-7e. Hodograph for merger-mode composite.

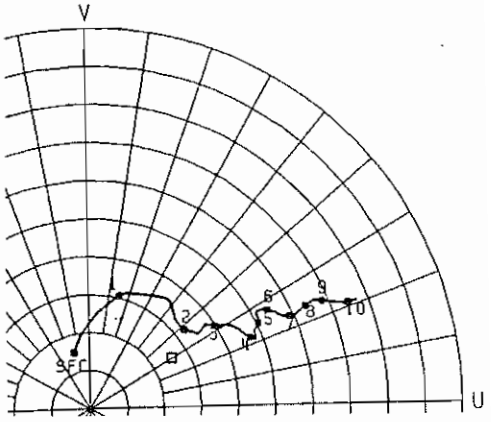

Fig. 3-7f. Hodograph for squall-line mode composite.

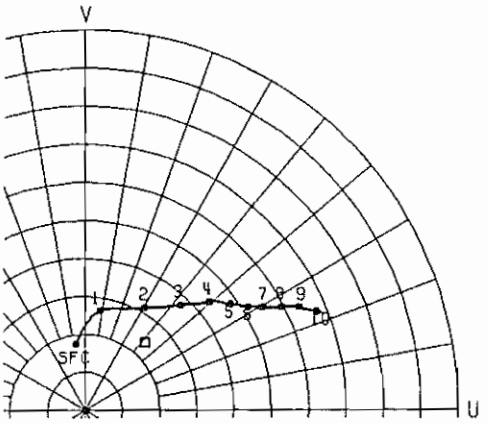

Fig. 3-37g. Overall composite hodograph.

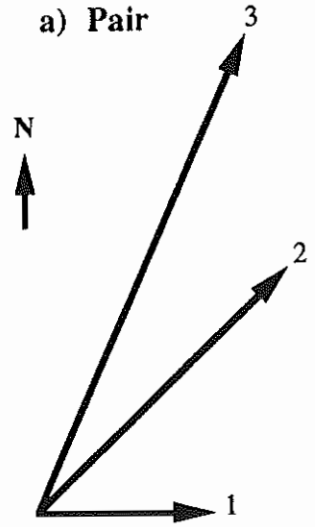

Fig. 3-8a. Orientations of initial cells in pair mode storms . Orientation "bins" are 22.5 degrees wide and are centered every 22.5 degrees starting at 360 degrees. Number of occurrences of each directional orientation shown by relative length of vector and plotted at end of vector.

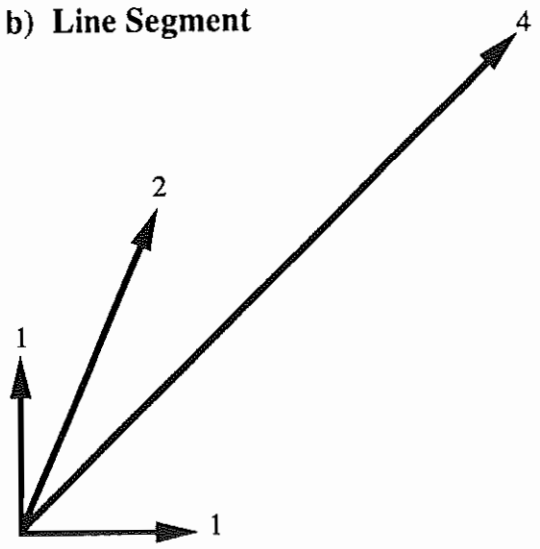

Fig. 3-8b. As in fig. 3-45a, but for line segment mode storms.

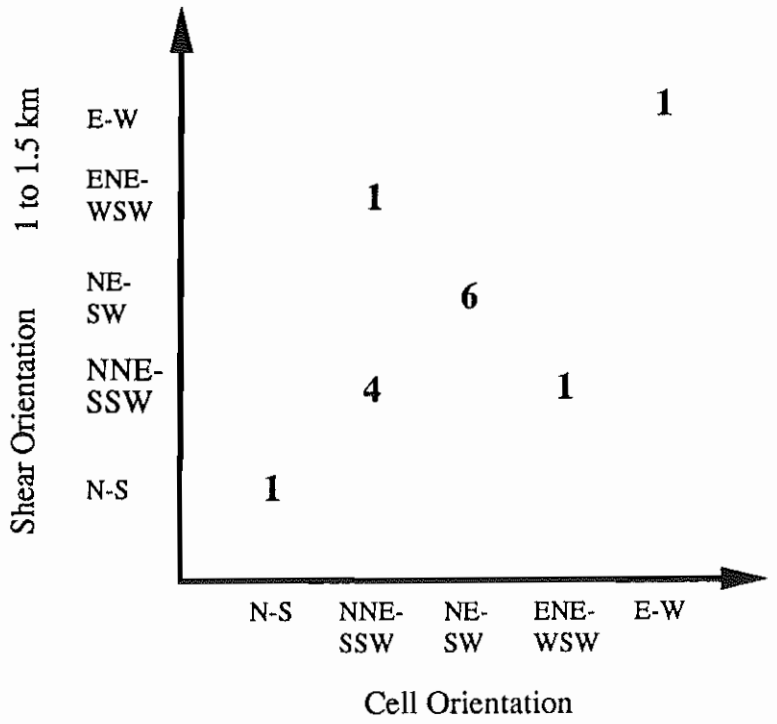

Fig. 3-9. Scattergram comparing orientations of initial cells of pair and line-segment mode storms with the shear vector in the 1 to 1.5 km AGL layer.

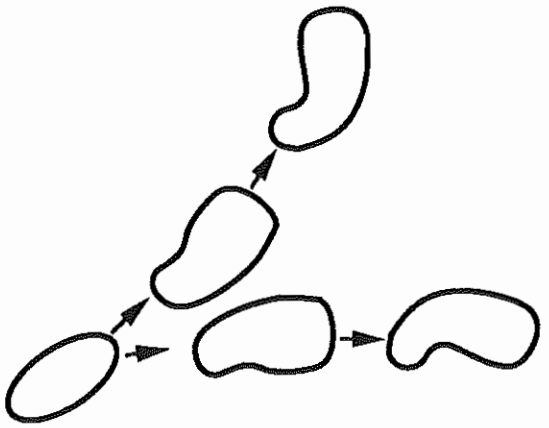

Fig. 3-10. Idealized splitting is depicted here for the case when both storms (right- and left-mover) become supercells. Each storm is approximately 20 km in diameter.

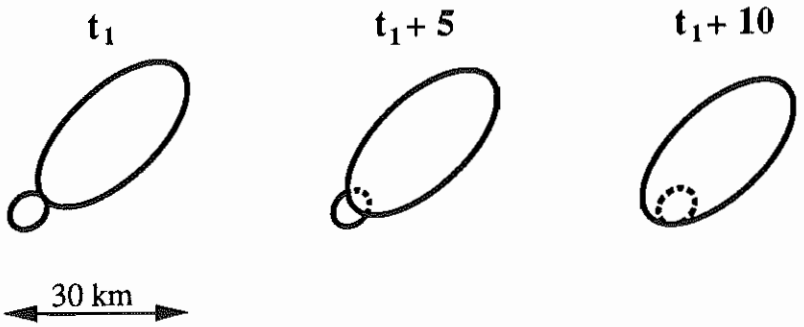

Fig. 3-11. Backbuilding is displayed in three steps. In step 1, a cell develops to (typically) the southwest of a storm in the study. Step 2 depicts the cell beginning to merge with the storm. Backbuilding is completed when the merger is complete, as shown in step 3. Sizes are relative. Representative horizontal scale is shown.

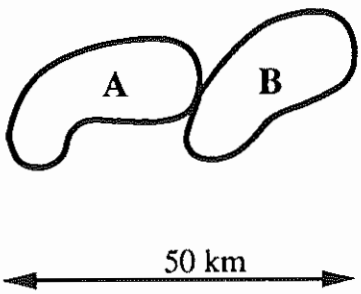

Fig. 3-12. The companion storm is this depiction is the storm labeled B. It is adjacent to storm A (representing a storm in the study) but does not merge with it. The two storms must remain this way for at least 20 minutes.

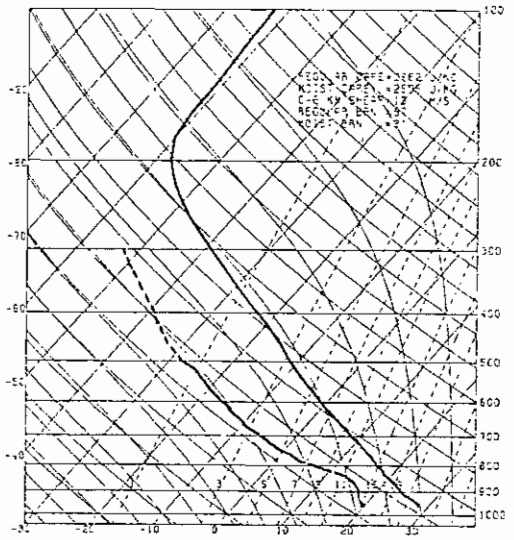

Fig. A-1. Sounding for composite of tornadic storms.

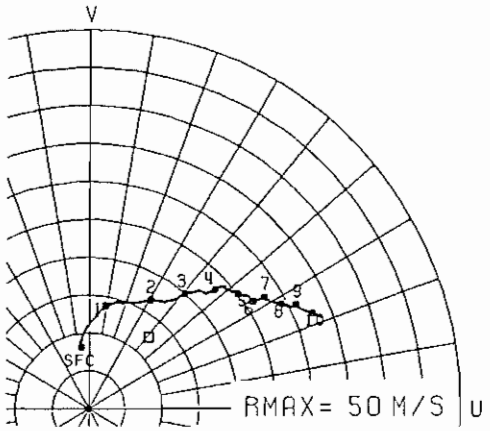

Fig. A-2. Hodograph for composite of tornadic storms.

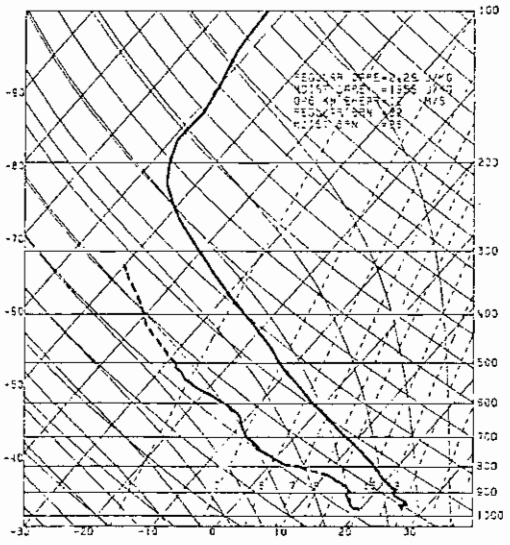

Fig. A-3. Sounding for composite of nontornadic storms.

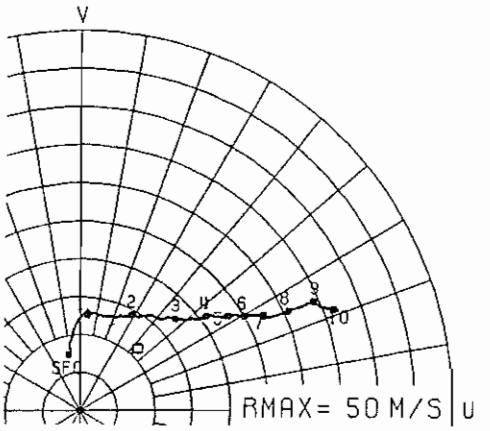

Fig. A-4. Hodograph for composite of nontornadic storms.